

**FULL PAPER**

# Green and chemical synthesis of bimetallic nanoparticles (Fe/Ni) supported by zeolite 5A as a heterogeneous fenton-like catalyst and study of kinetic and thermodynamic reaction for decolorization of reactive red 120 dye from aqueous pollution

Maysoon M. Abdul Hassan<sup>a,\*</sup>  | Sahar S. Hassan<sup>b</sup> | Ahmed K. Hassan<sup>a</sup><sup>a</sup>Environment and Water Directorate, Ministry of Science and Technology, Baghdad, Iraq<sup>b</sup>Department of Chemistry, College of Science for Women, University of Baghdad, Baghdad, Iraq

In this work, the green and chemical synthesis of bimetallic nanoparticles (Fe/Ni) NPs supported by zeolite 5A using green tea extract and sodium borohydride as reducing agents, respectively, at the best ratio of Fe: Ni was obtained and used as heterogeneous Fenton-like oxidation for the decolorization of reactive red 120 dye (RR120) from water polluted. The nanoparticles were characterized by using SEM, (EDX), (AFM), (XRD), (FT-IR), (BET), and Zeta potential. The hydrothermal preparation of zeolite 5A from local kaolin, then characterization, and use of it as a supporting material. The optimum conditions of decolorization of RR120 were studied under experimental parameters such as:  $[H_2O_2] = (0.1-20)$  mmol/L, catalyst dosages =  $(0.1-1.5)$  g/L, pH  $(2.5-9)$ ,  $[RR120 \text{ dye}] = (15-100)$  mg/L, reaction time =  $(0-120)$  min, and temperature  $(30-50)$  °C. The decolorization efficiency of RR120 dye under the optimum reaction conditions by Fenton-like reaction for (GT-Z-Fe/Ni) NPs synthesis by green methods was 99.9%, whereas 96.6% with (Z-Fe/Ni) NPs synthesized by chemical methods. Furthermore, we studied the kinetic and thermodynamic effects of RR120 dye removal by heterogeneous Fenton-like oxidation for GT-Z-Fe/Ni and Z-Fe/Ni NPs by three kinetic models (first-order, second-order, and Behnajady-Modirshahla-Ghanbary (BMG)) and the thermodynamic parameters ( $\Delta G^0$ ,  $\Delta H^0$ , and  $\Delta S^0$ ) at  $(30, 40, \text{ and } 50)$  °C. The results indicate the second-order and the (BMG) are the best models representing the experimental kinetic data of RR120 dye removal, and the reaction is spontaneous and endothermic using GT-Z-Fe/Ni and Z-Fe/Ni nanoparticles. Finally, the comparison of the decolorization efficiency of RR120 dye in optimum conditions using different reaction mechanisms.

**\*Corresponding Author:**

Maysoon M. Abdul Hassan

Email: [maysoon\\_mzahir@yahoo.com](mailto:maysoon_mzahir@yahoo.com)

Tel.: +947730015951

**KEYWORDS**

Green synthesis; chemical synthesis; Fenton-like oxidation; bimetallic Fe/Ni nanoparticles; zeolite-supported nanoparticles; azo dyes.

**Introduction**

The most severe form of water pollution in developing countries is the uncontrolled release of hazardous and persistent organic

compounds into aquatic systems [1]. Various industries generate waste that is discharged into water effluents, affecting the appearance and quality of water and causing a severe

problem by reducing the amount of pure and clean water available in our world. The organic pollutants, particularly dyes, are among these wastes, and they have a harmful effect on the environment and humans [2]. The azo dye-containing wastewater discharged has a high level of environmental toxicity, is non-biodegradable, poses a risk to human health and the aquatic ecosystem as well as it has the potential to cause cancer in humans [3]. Various materials and techniques, such as adsorption, electrocoagulation, phytoremediation, membrane separation, and advanced oxidation processes (AOPs) have been utilized to remediate industrial water contaminated with dyes [4]. AOPs are widely used to eliminate complex organic contaminants [5,6]. The environmentally benign approach of AOPs is heterogeneous Fenton oxidation, which is based on the reaction of solid iron (as a catalyst) with hydrogen peroxide ( $H_2O_2$ ) to form highly reactive intermediate species known as hydroxyl free radicals [7]. The advantages of using this method are that it has the highest efficiency of dye removal, is more feasible, and is not expensive as compared with a homogeneous one [5]. In the green Fenton-like oxidation process, hydroxyl radicals are produced by a green synthesis of metal-catalyzed oxidation using hydrogen peroxide and then consumed to remove azo dyes [6,8]. Chemical methods used in the production of iron nanoparticles by using materials such as sodium borohydride or hydrazine hydrate, cause increased toxicity in the environment and have detrimental effects on living organisms [9] and several drawbacks, including reliance on expensive equipment, significant energy consumption and a reliance on chemical substances that are hazardous to the environment and individuals. Green synthesis is another eco-friendly approach which avoids the use of harmful chemicals. Because it uses biological microorganisms or plant extracts, green synthesis has become a

simple alternative to toxic chemical techniques. It is also environmentally benign, cost-effective, and easy to scale up to large-scale synthesis for metal ion bioreduction [10]. Plant extracts have been widely used to reduce the negative impacts of chemical synthesis, and they have a significant advantage due to their natural abundance, low cost, eco-friendliness [9], and large surface area [11]. Although iron nanoparticles have achieved the broad usage as a promising metal in treatment methods for the removal of a variety of environmental contaminants, their reactivity may be affected by the formation of an oxide layer around particle surfaces. Due to its aggregation feature and ease of oxidation on the surface, a second catalyst such as Cu, Pt, Pd, or Ni can be added to improve catalytic reactivity and reduce iron oxidation [12]. Because the mutual action of two metals improves the properties of nanoparticles as compared with using only one metal (monometallic). In an NZVI-based bimetallic system, the iron acts as an electron donor, while the second metal acts as both a carrier and a catalyst, accelerating the transition of H into activated atomic H, and thereby enhancing NZVI's reduction reactivity [13]. Although Ni had a weak catalytic effect when compared with noble metals like Pd and Pt, it was more useful for practical applications due to its inexpensive cost and strong corrosion resistance [14]. The stabilization of bimetallic nanoparticles into suitable support materials is needed to overcome the limitations of bimetallic nanoparticles [14]. Biochar, montmorillonite, rectorite, bentonite, kaolinite, zeolite, and sepiolite, are examples of supporting materials that improve not only the dispersion of NZVI particles, but also their reactivity by acting as pre-concentrate reactants and mediating electron transfer reactions [15]. Supporting materials like zeolite, as a microporous material, have unique physicochemical properties, such as the presence of strong acidic centers, an

extremely large surface area, high ion-exchange ability, and a precise system of micropores and channels, all of which could improve NZVI dispersibility and stability [15].

In this work, bimetallic GT-Z-Fe/Ni and Z-Fe/Ni nanoparticles were synthesized in different ratios of Fe/Ni using green tea leaf extract and sodium borohydride as a reducing agent. Then, these ratios were evaluated to select the most effective ratio for removing reactive red 120 dye (RR120), which is an example of an azo dye. The goals of this study are: (1) using zeolite 5A as supporting material for bimetallic Fe/Ni nanoparticles to improve the reaction of nanoparticles, reduce the cost, and enhance the adsorption capacity for nanoparticles; (2) to investigate the functions of bimetallic GT-Z-Fe/Ni and Z-Fe/Ni NPs in heterogeneous Fenton-like oxidation; (3) to investigate the influence of various parameters on the degradation rate of the RR120 dye from aqueous solution; (4) to assess the effect of three kinetic models and thermodynamic reaction parameters on the degradation of RR120 dye by using bimetallic NPs and (5) to compare the decolorization efficiencies of RR120 dye with Fenton-like oxidation and adsorption processes by using catalysts bimetallic GT-Z-Fe/Ni and Z-Fe/Ni NPs and zeolite 5A under optimum conditions.

## Experimental procedure

### Instrumentation

The field emission scanning electron microscope FE-SEM (TESCAN MIRA3, FEG-SEM) (1-30 kV) (Franch) is a type of high-resolution electron microscopy that produces three-dimensional digital images, this model was used to investigate the morphology, topography, and average particle size. The SEM images were taken to identify bimetallic (GT-Z-Fe/Ni) and (Z-Fe/Ni) nanoparticles and to identify changes in the surface morphology. The electron dispersive x-ray spectroscopy (EDX) XFlah6-10 Detector-

Bruker is used to identify the elemental composition of nanoparticles. The size and surface morphology of the nanoparticles, as well as the contact force between the tip and the surface, were measured using an atomic force microscopy (AFM) model (AFM Workshop, TT-2AFM) (USA). The surface composition and element combination state of bimetallic [GT-Fe/Ni and Z-Fe/Ni] nanoparticles were studied using an x-ray diffraction (XRD) model (Panalytical X'Pert Philips, Holland), Brunauer-Emmett-Teller (BET) (Micromeritics TriStar II Plus 2.03) (USA) at analysis adsorptive, the surface area was determined using a Brunauer-Emmett-Teller (BET) (Micromeritics TriStar II Plus 2.03) (USA) at N<sub>2</sub> temperature in the bath (-196.675 °C) to calculate the specific surface area (BET), pore-volume, and average pore size of GT-Z-Fe/Ni and Z-Fe/Ni by using a sample mass of 0.1515 g of GT-Z-Fe/Ni and Z-Fe/Ni transferred to the BET tube. Each of these items was analyzed in the laboratory of Kashan University (Iran). A zeta potential analyzer model (NanoBrook ZetaPlus) was utilized to determine nanoparticle stability by studying the electrophoretic behavior of the fluid. The zeta potential of any nanoparticle might be positive at low pH levels and negative at high pH levels. The zeta potential that was measured had a pH of about 6. An FT-IR spectroscopic instrument was used to determine the functional groups present on the GT-Z-Fe/Ni and Z-Fe/Ni (Shimadzu, Japan in the 400 to 4000 cm<sup>-1</sup> range). This was carried out in the laboratories of Iraq's Ministry of Science and Technology's Environment and Water Directorate. The concentration of RR120 dye in an aqueous solution before and after treatment was analyzed by a UV-Vis Spectrophotometer (Optima, SP-3000 Plus, Tokyo, Japan) at a maximum absorption wavelength of 535 nm and pH (pH meter, WTW, Germany). Shaking Water Bath B5-21, JEIO TECH (Korea). Ultrasonic Cole-Parmer, Four Digital Balances and Magnetic Stirrers, ABINCO.LD-814

(Netherlands), SCIEN TECH, BOULDER.COM (USA), and Heidolph (RZR1) mechanical stirring (Germany).

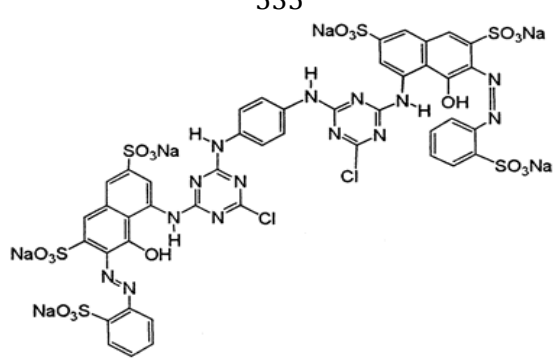
## Materials and methods

### Materials and solutions

All of the utilized reagents were of the highest purity and provided without further purification. Deionized water of the highest purity was used to make all of the solutions. The kaolin clay used in the present work was supplied from the Doakhla site in the west of Iraq. The green tea leaves were purchased

from the local market. Hydrogen peroxide ( $\text{H}_2\text{O}_2$ ) at 30% weight per weight, ferrous sulfate heptahydrate ( $\text{FeSO}_4 \cdot 7\text{H}_2\text{O}$ ), nickel nitrate hexahydrate ( $\text{NiNO}_3 \cdot 6\text{H}_2\text{O}$ ), and ethanol from BDH. Sodium borohydride ( $\text{NaBH}_4$ ) from Merck & Co. (Germany). Sodium hydroxide ( $\text{NaOH}$ ) and sulfuric acid ( $\text{H}_2\text{SO}_4$ ) were used to adjust pH and were purchased from Appli Chem (GbH). The Reactive Red 120 dye was a gift from the Textile Factory from the Ministry of Industry and Minerals. The commercial reactive red 120 dye's main characteristics and chemical structure have been described in Table 1.

**TABLE 1** The Commercial Reactive Red 120 dye's main characteristics and chemical structure

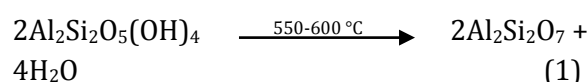
<b>IUPAC Name</b>	Hexasodium 4,4'-[1,4-phenylenebis[imino(6-chloro-1,3,5-triazine-4,2-diy)]imino]]bis[5-hydroxy-6-[(2-sulphonatophenyl)azo]naphthalene-2,7-disulphonate]
<b>Common Name</b>	Reactive Red 120
<b>Dye Glass</b>	Diazo
<b>Molecular formula</b>	$\text{C}_{44}\text{H}_{24}\text{Cl}_2\text{N}_{14}\text{Na}_6\text{O}_{20}\text{S}_6$
<b>Molar Mass</b>	1470 g/mol
<b>Application:</b>	Reactive red 120 is a polyaromatic azo organosulfur dye
<b>Purity</b>	98.8
<b>Color</b>	Bright Red
<b><math>\lambda</math> max (nm)</b>	535
<b>Chemical Structure</b>	

### Synthesis of zeolite-Fe/Ni nanoparticles by green and chemical methods

#### Preparation of zeolite 5A

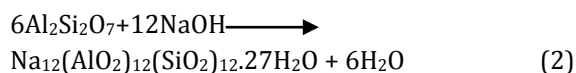
To prepare the zeolite 5A, kaolin clay was taken from the Dwikla site. The local kaolin clay was crushed and sifted to 75-micron grain size. To produce zeolite 4A from kaolin clay by thermal activation of kaolin clay and ion exchange methods. Metakaolin is produced through the thermal activation of kaolin clay. The dried kaolin clay was calcined

at 550 °C for 3 hours. As illustrated by the following reaction:



Through ion exchange, the sodium ion was inserted into the kaolin structure by treating it with sodium hydroxide. In a 1:2 ratio, meta kaolinite was treated with a sodium hydroxide solution. The meta kaolinite (0.1 M, 2.22 g) was treated with a sodium hydroxide solution (0.2 M, 8 g) in 100 mL of

distilled water and then refluxed for 8 hours in a shaker water bath at 95 °C. Zeolite was left to settle for several hours and washed three times with deionized water to remove the excess on the reacted sodium hydroxide. Then, it was filtered by any suitable means and dried in an oven at 110 °C for four hours. The following reaction led to the preparation of zeolite 4A.



Ion exchange was used to produce zeolite type 5A from zeolite type 4A. Calcium ( $\text{Ca}^{+2}$ ) ions were replaced by sodium ions in zeolite type 4A. They were produced by reacting 25 g of zeolite type 4A with a 1M  $\text{CaCl}_2$  solution (22.19 g of  $\text{CaCl}_2$  (1M) in 200 mL of distilled water). The solution was then filtered and dried for 4 hours at 110 °C in an oven. As for zeolite type 5A, the obtained zeolite powder was ground, molded, and calcined. The chemical analysis of the synthesized zeolite 5A was conducted at 95 °C and 8 hours of shaking. Because of its high surface area and pore size [16], we chose zeolite 5A to synthesize zeolite-supported nanoparticles.

#### *Synthesis of zeolite-Fe/Ni nanoparticles (GT-Z-Fe/Ni) by green methods*

##### *Preparation of green tea extraction*

The green tea extract was produced by mixing 10.0 g of green tea in 100 mL of deionized water on the hot plate. The solution was heated for 30 min at 85 °C. The extract was filtered through a 0.45 m membrane filter to remove the remaining tea particles and kept at 4 °C for later usage as reducing agent.

##### *Synthesis of green Tea-Z-Fe/Ni (GT-Z-Fe/Ni) nanoparticles*

A solutions of (0.10 M)  $\text{FeSO}_4 \cdot 7\text{H}_2\text{O}$  and (0.01M)  $\text{NiNO}_4 \cdot 6\text{H}_2\text{O}$  was prepared in the best ratio (1:0.2) of Fe:Ni by adding 4.9782 g and 0.77928 g, respectively, of solid  $\text{FeSO}_4 \cdot 7\text{H}_2\text{O}$

and  $\text{NiNO}_3 \cdot 6\text{H}_2\text{O}$  to 178 mL of deionized water. After complete dissolving, this solution was filtered using a 0.45  $\mu\text{m}$  membrane filter to remove any impurities. The solutions of  $\text{FeSO}_4 \cdot 7\text{H}_2\text{O}$  and  $\text{NiNO}_3 \cdot 6\text{H}_2\text{O}$  were mixed, and then they were stirred immediately for 30 min at room temperature at 300 pm. Then 2.0 g of the zeolite (5A) was added to this solution and stirred for 60 min in an ultrasonic vibration bath where the best ratio of zeolite: Fe:Ni was **2:1:0.2** (w/w). Then, dropwise, the green tea extract was added to the mixture of  $\text{FeSO}_4 \cdot 7\text{H}_2\text{O}$ ,  $\text{NiNO}_3 \cdot 6\text{H}_2\text{O}$ , and zeolite 5A solutions by adding it slowly for 15 min at room temperature and immediately stirring it at 300 pm. After the addition, the color of the solution changed from yellowish-green to black, which indicated the reduction of iron (II) ions to iron (0) nanoparticles. Constantly stirred for 15 min, the black precipitate of GT-Z-Fe/Ni nanoparticles was collected by vacuum filtration using filter paper of 0.45  $\mu\text{m}$  pore size and quickly rinsed several times with water and ethanol. The GT-Z-Fe/Ni nanoparticles were dried at 50 °C in an oven and then ground to a fine powder.

#### *Synthesis of zeolite-Fe/Ni (Z-Fe/Ni) nanoparticles by chemical method*

The Z-Fe/Ni nanoparticles were prepared by the liquid-phase reduction method using sodium borohydride as a reducing agent. The solutions of (0.10 M)  $\text{FeSO}_4 \cdot 7\text{H}_2\text{O}$  and (0.01M)  $\text{NiNO}_4 \cdot 6\text{H}_2\text{O}$  were prepared in the best ratio (1:0.2) of Fe:Ni by adding 4.9782 g and 0.77928 g, respectively, of solid  $\text{FeSO}_4 \cdot 7\text{H}_2\text{O}$  and  $\text{NiNO}_3 \cdot 6\text{H}_2\text{O}$  to 178 mL of deionized water. After complete dissolving, this solution was filtered using a 0.45  $\mu\text{m}$  membrane filter to remove any impurities. The solutions of  $\text{FeSO}_4 \cdot 7\text{H}_2\text{O}$  and  $\text{NiNO}_3 \cdot 6\text{H}_2\text{O}$  were mixed in a three-neck flask and stirred by a mechanic stirring put inside the flask for 30 min at 300 rpm at room temperature. Then 2.0 g of the zeolite (5A) was added to this solution at the best ratio of zeolite: Fe: Ni



ratio of 2:1:0.2 (w/w) was chosen and stirred for 60 minutes in an ultrasonic vibration bath.  $N_2$  gas flowed into the three-neck flask from the beginning of the reaction and continued throughout the reaction. The sodium borohydride  $NaBH_4$  (0.3 M) aqueous solution was prepared by dissolving (1.13403 g) in 100 mL of deionized water in a separation flask inside a three-neck flask, then adding dropwise (5 mL per minute) to the solution of  $FeSO_4 \cdot 7H_2O$ ,  $NiNO_3 \cdot 6H_2O$ , and zeolite, and immediately stirring for 30 minutes at room temperature at 300 rpm. The color of the solution changed from yellowish-green to black, indicating the reduction of iron (II) ions to iron (0) nanoparticles, with the continued flow of  $N_2$  gas into the three-neck flask for the reaction to end, removing the air and avoiding oxidation of the nanoparticles formed. The black precipitate of Z-Fe/Ni nanoparticles was collected by vacuum filtration using filter paper of 0.45  $\mu m$  pore size and quickly rinsed several times with water and ethanol, keeping it immediately in ethanol or methanol solution.

#### *Selection of the optimum ratio of Fe/Ni*

The experiments for the Fe/Ni (1: 1, 1: 0.5, and 1: 0.2) ratios were carried out at different pH (2.5-9) and the results revealed that the 1:0.2 ratio has a higher level of removal efficiency than the 1:1 and 1:0.5 ratios. The rapid increase in RR120 removal was noticed in the first 30 min and that was due to the availability of active sites on the adsorbent surface that adsorbed a large amount of dye. Then the removal rate slowed because we are approaching the saturation of vacant sites. After selection of the highest percentage, the removal of RR120 dye among Fe/Ni (1:1, 1:0.5, and 1:0.2) and then the characterization of the best ratio of GT-Fe/Ni and Z-Fe/Ni NPs were conducted.

#### *Batch experiments procedure*

In this search, batch experiments were carried out to determine the removal efficiency of RR120 dye using the following approach. Dye removal experiments were carried out in 1000 mL beakers with 1000 mL of dye solution of the desired concentration. The effect of the concentration of  $H_2O_2$  on heterogeneous Fenton-like oxidation ranges from (0.1-7.5) mmol/L in the state of bimetallic GT-Z-Fe/Ni NPs and (0.1-20) mmol/L in the state of bimetallic Z-Fe/Ni NPs on the elimination of RR120 dye solution (25 g/L) was tested at a pH =3 using the GT-Z-Fe/Ni and Z-Fe/Ni dose (0.2 and 0.5) g/L respectively. The concentration of RR120 dye during Fenton-like oxidation was measured by taking 10 mL samples at predetermined intervals, filtering the samples with 0.45  $\mu m$  pore size membrane filters to remove the catalyst, and transferring the samples to a glass vial. The effect of GT-Z-Fe/Ni and Z-Fe/Ni nanoparticles dosages in the range of (0.05-1.5) g/L on the degradation of 1 L of a synthetic solution with 25 mg/L RR120 dye at a fixed  $H_2O_2$  concentration of (1 and 7.5) mmol/L, respectively and pH=3 was investigated in Fenton-like experiments. Subsequently, the experiments were carried out at pH values ranging from (2.5 to 9.0) to find the optimal pH for RR120 dye degradation. Meanwhile, under optimal conditions condition of pH, GT-Z-Fe/Ni and Z-Fe/Ni dose and concentration of  $H_2O_2$  in heterogeneous Fenton-like oxidation on the elimination of RR120 dye solution the initial concentration of RR120 dye was tested in the range of (15-100) mg/L and the reaction temperature was estimated to be between (30-50) $^{\circ}C$ . At specific time intervals (5, 10, 15, 20, 30, 45, 60, 90, and 120) min, the RR120 dye concentration was analyzed in the solution.

### Analytical methods of RR120 dye aqueous media

Organic compounds such as RR120 dye solution of desired concentration were prepared by dilution of stock solution instantly before use. Stock solutions of RR120 dye were prepared in demineralization water. Figure 1 displays the calibration curve for RR120 dye concentrations at  $\lambda_{\max}=535$  nm wavelength. The absorbance of the RR120

dye solution was measured before and after degradation by using a UV-Vis spectrophotometer (model SP-3000 OPTIMA, Japan) equipped with a quartz cell of 1.0 cm Path length. The decolorization efficiency ( $E_d$ ) (%) for RR120 dye was expressed in terms of the decrease rate in the dye concentration, it was calculated as in Equation(3), where  $C_0$  is the initial concentration of RR120 dye, and  $C_t$  is the concentration of RR120 dye at time  $t$ .

$$E_d\% = [C_0 - C_t / C_0] \times 100\% \quad (3)$$

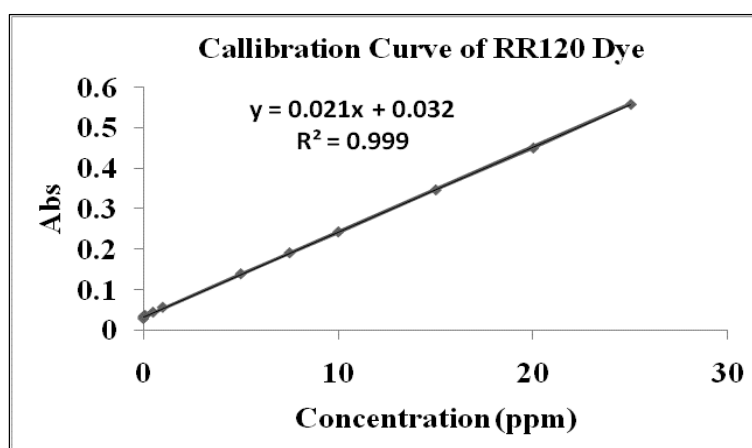


FIGURE 1 Calibration curve for RR120 dye concentrations at  $\lambda_{\max}=535$  nm

## Results and discussion

### Characterization of bimetallic nanoparticles

#### Scanning electron microscope (SEM)

The scanning electron microscope (SEM) is a direct method for determining nanoparticle size and surface morphology. It is used to investigate the morphology, topography, and average particle size. The external appearance, texture, chemical composition, crystalline structure, and orientation of components which make up the sample are all revealed by the signals derived from electron sample interactions [17]. The morphology and size of the synthesized [GT-Z-Fe/Ni and Z-Fe/Ni] NPs samples were verified using SEM, which was utilized to assess the diameter of the nanoparticles as illustrated in Figure 2. The morphology and distributions of GT-Z-Fe/Ni NPs Figure 2A in SEM images revealed that synthesized GT-Z-

Fe/Ni NPs were uniformly dispersed on the surface of zeolite with no aggregation, and these nanoparticles were porous and shaped as spherical, with diameters ranging from (24-36) nm, indicating that Fe/Ni NPs were present on the surface of zeolite, they were well-supported. Therefore, as depicted in SEM images in Figure 2B, chemically synthesized Z-Fe/Ni NPs morphology and distributions were uniformly dispersed on the surface of zeolite with no aggregation and a uniform size of (29-52) nm. Because zeolite disperses and stabilizes (Fe/Ni) NPs, it helps to minimize costs, maximize the adsorption capacity of Fe/Ni and increase the surface area and active sites for reactivity enhancement, it was chosen as a support material. The zeolite is thought to minimize the aggregation propensity of nanoparticles caused by the magnetic characteristics of iron nanoparticles while also protecting them from oxidation [18]. The presence of

polyphenols on the surface of the GT-Z-Fe/Ni NPs resulted in irregular nanoparticle morphologies, which was confirmed by NZVI preparation results by using tree leaf extract and green tea extract. This is dependent on the number of polyphenols in the extract,

which can produce a variety of reactions, such as inhibiting or stimulating the formation of GT-Z-Fe/Ni nanoparticles, resulting in a variety of forms and sizes of iron nanoparticles [6].

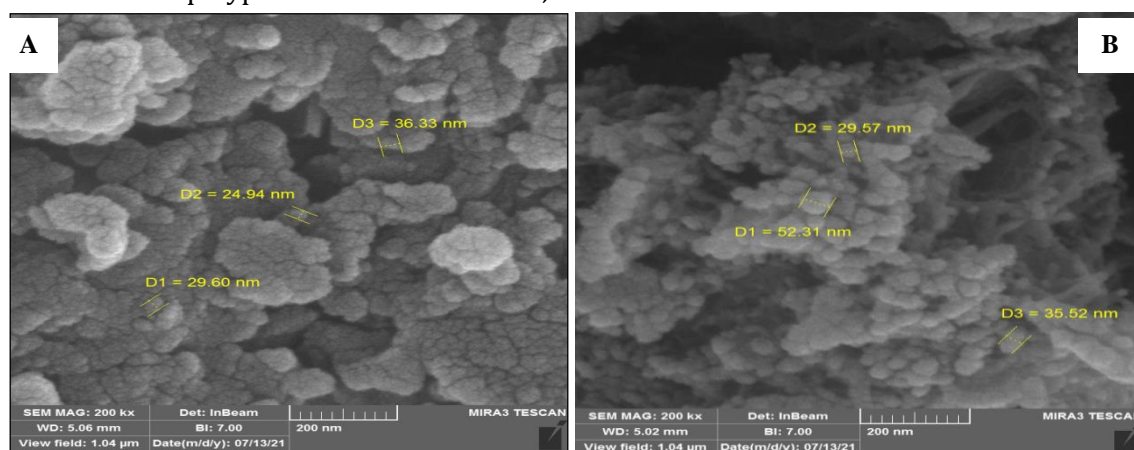
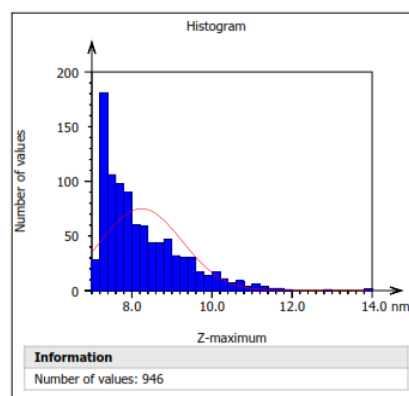
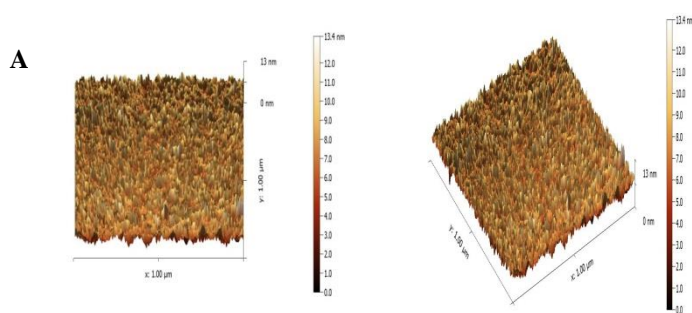


**FIGURE 2** Scanning electron microscope images of bimetallic NPs (A)- GT-Z-Fe/Ni and (B)- Z-Fe/Ni

#### Atomic-force microscopy

Atomic force microscopy (AFM) is used to analyze the topography of nanomaterials. The attracted or repulsive forces between a nanometer-sized fine tip (20–50 nm) or less and the substance are measured using AFM [19]. The AFM studies were used to analyze the diameter of the nanoparticles and were used to verify the morphology and size of the synthesized [GT-Fe/Ni and Z-Fe/Ni] samples. The high rough surface was formed by hills and valleys shaped with a nano-rough texture

and homogenous distribution of NPs as indicated in Figure 3. This roughness enhances the capability of the NPs surface to absorb the ions. The average size distribution of particles of GT-Z-Fe/Ni synthesized iron nanoparticles tested by AFM is an average diameter of less than 8.243 nm, as shown in Figure 3A, and Z-Fe/Ni had an average diameter of less than 61.46 nm and no agglomeration, as displayed in Figure 3B.





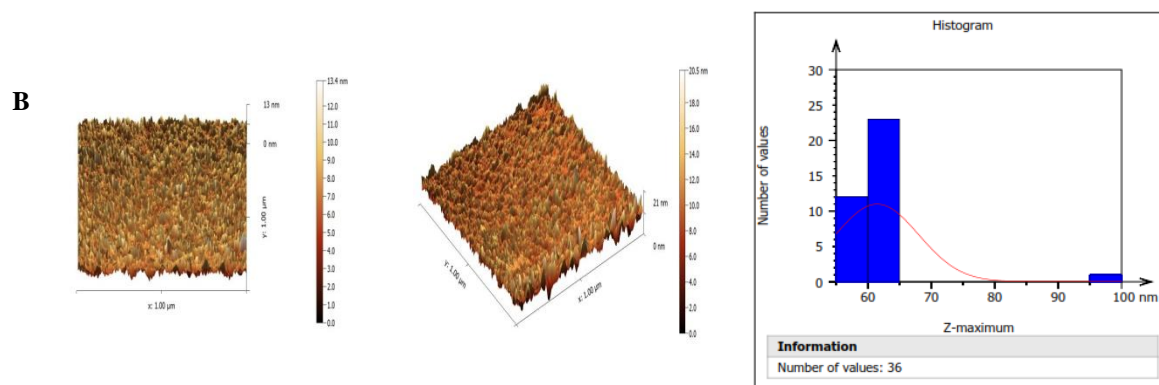


**FIGURE 3** Atomic Force Microscopy (AFM) images of (A): GT-Z-Fe/Ni and (B): Z-Fe/Ni

### Energy-dispersive spectroscopy

The energy-dispersive spectroscopy (EDXS) technique is a confirmatory technique for verifying particle identification, chemical classification, and the elemental composition of nanoparticles can be determined. Figure 4 depicts the energy dispersive X-Ray spectroscopy (EDXS) spectrum of nanoparticles, which offers information about the synthesis of GT-Fe/Ni and Z-Fe/Ni NPs, such as the location of atomic distribution on the surface and chemical composition of (GT-Z-Fe/Ni and Z-Fe/Ni) NPs. The intense peaks

of (Fe, Ni, C, O, Al, and Si), 3.05 wt%, 1.08 wt%, 50.00 wt%, 40.00 wt%, 2.98 wt%, and 2.88 wt%, respectively in the GT-Z-Fe/Ni NPs and the intense peaks of (Fe, Ni, C, O, Ca, Al, and Si), 2.04 wt%, 1.04 wt%, 12.92 wt%, 60.40 wt%, 3.67 wt%, 6.66 wt%, and 13.27 wt%, respectively in the analysis of Z-Fe/Ni NPs. The discovery of adjoining elements like C and O signals was primarily due to the green tea extracts, C and O are organic substances which play an important role in the reduction and stabilization of GT-Fe/Ni NPs [20,21].

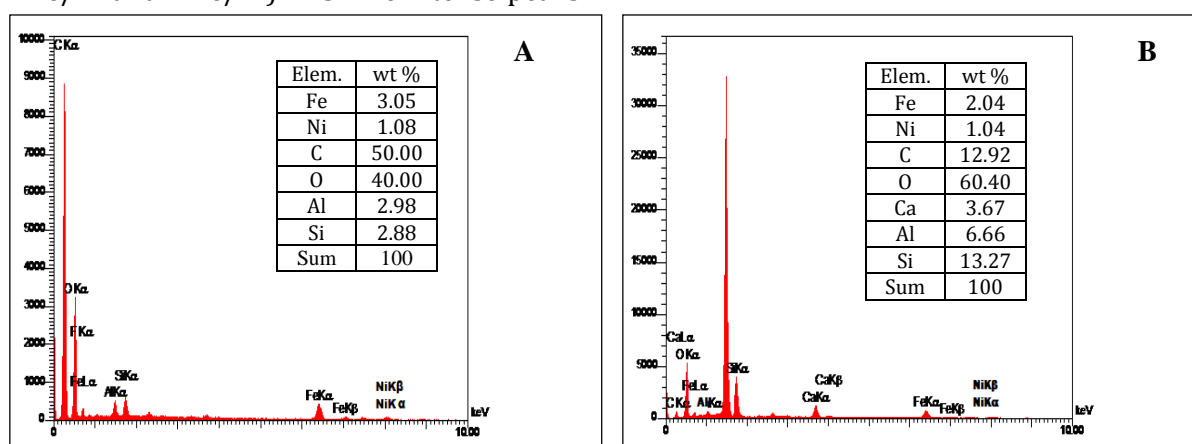


**FIGURE 4** EDAX of prepared (A)- GT-Z-Fe/Ni and (B)- Z-Fe/Ni NPs samples

### X-Ray diffraction

The morphology of nanoparticles is widely studied using X-ray diffraction. The diffraction pattern produced by XRD is then compared to data in a standard crystallographic database. According to Bragg's law, the findings of an X-ray

diffraction test were used to calculate the d-spacing of NPs. The relationship between intensity and diffraction angle  $2\theta$  in Bragg's law ( $n = 2d \sin \theta$ ) is depicted in the x-ray diffraction figure. The Debye-Scherrer equation ( $t = K \lambda / \beta_c \cos \theta$ ) is used to calculate the crystallite size of a sample from the FWHM of a diffraction peak broadening.

Where the crystallite size is  $t$ ,  $\beta_c$  is the FWHM, and  $(K)$  is the Scherrer's constant, which varies between 0.9 and 1.15 for diffractions with varying crystallographic Miller indices  $(hkl)$  of a cubic crystal lattice and it is usually assumed to be 0.9 for cubic materials for simplicity. The X-ray diffraction (XRD) of the [GT-Z-Fe/Ni] and [Z-Fe/Ni] NPs nanoparticles synthesis by green and chemical methods as demonstrated in Figure 5A and B, the number of diffracting planes is limited therefore, the diffraction peak will broaden significantly (from  $10^\circ$ - $70^\circ$ ) due to the insufficient number of planes causing destructive interference at the diffraction angles other than Bragg's angle. The XRD diffraction pattern exhibited the obvious peaks at  $2\theta$   $44.8^\circ$  and  $65.0^\circ$ , which belong to  $Fe^0$  in GT-Z-Fe/Ni and Z-Fe/Ni NPs confirming the existence of Fe/Ni NPs on the zeolite surface. Furthermore, a very small peak that belongs to iron oxide  $Fe_2O_3$  ( $2\theta$

$=35.6^\circ$ ) and  $Fe_3O_4$  ( $2\theta=35.7^\circ$ ) was also observed, indicating that only a small portion of the NZVI particles was oxidized in GT-Z-Fe/Ni using green tea extract as a reducing agent instead of sodium borohydride. Because it has good oxidation resistance, in addition to using supported zeolite that dispersed them uniformly. Hence, as in Z-Fe/Ni NPs synthesis by chemical approach, the zeolite reduces the oxidation [22]. The pattern indicated the typical peaks of Ni ( $2\theta=44.2^\circ$ ),  $Ni(OH)_2$  ( $2\theta=30.8^\circ$ ), and  $FeO(OH)$  ( $2\theta=30.0^\circ$ ). The diffraction peaks at  $2\theta=(10^\circ-30^\circ)$  were attributed to a zeolite structural feature. Figure 5C reveals that zeolite type 5A has a high degree of crystalline and contains some quartz. The characteristic peaks of the prepared zeolite type 5A are at the angle ( $2\theta=7.3^\circ$ ) with an intensity of 2500, at ( $2\theta=26^\circ$ ) with an intensity of 2000, and at ( $2\theta=27^\circ$ ) with an intensity of 850.

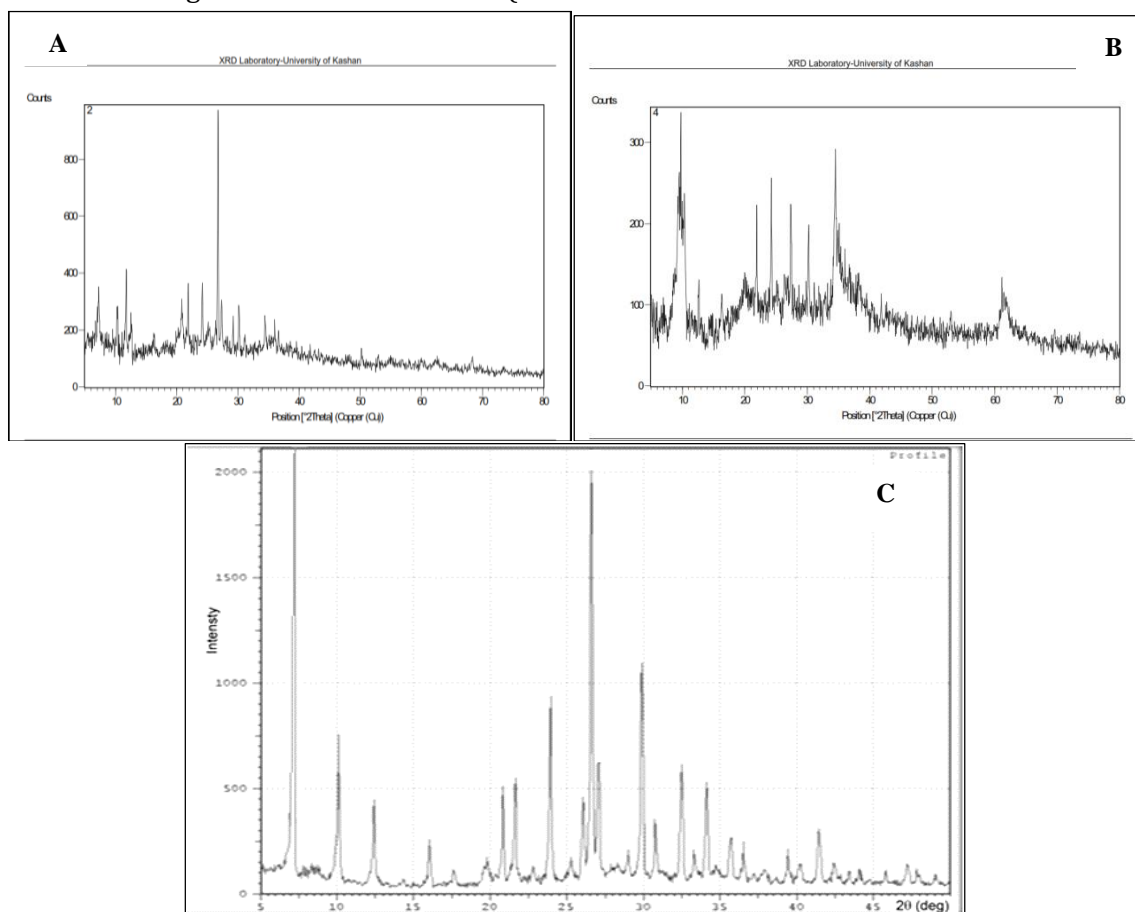


**FIGURE 5** X-ray Diffraction (XRD) images of (A): GT-Z-Fe/Ni and (B): Z-Fe/Ni(C): Prepared Zeolite 5A

*Brunauer-Emmett-Teller (BET)*

The specific surface area (BET), pore volume, average pore size, and Langmuir surface area of synthetic zeolite 5A and (GT-Z-Fe/Ni and Z-Fe/Ni) nanoparticles are listed in Table 2. When zeolite 5A was compared to zeolite supported on Fe/Ni (GT-Z-Fe/Ni) and (Z-Fe/Ni), the specific surface area decreased from 221.10 m<sup>2</sup>/g to (18.47 and 32.72) m<sup>2</sup>/g, pore volume decreased from 0.15 cm<sup>3</sup>/g to (0.05 and 0.10) cm<sup>3</sup>/g and average pore size increased from 2.73 nm to (11.54 and 12.76) nm, respectively. The decrease in specific surface area and pore volume was most commonly caused by nanoscale Fe/Ni particles loading zeolite pores, whereas the increase in average pore size could be due to micropore clogging [15]. When Fe/Ni particles were loaded onto zeolite, they had a significantly greater surface area, pore-volume and decreased pore size, indicating that zeolite played an important role in dispersing Fe/Ni and therefore increasing the surface area and active sites for reactivity improvement. These bimetallic [GT-Z-Fe/Ni and Z-Fe/Ni] nanoparticle results revealed an improvement in nanoparticle structure because the presence of zeolite leads to an increase in surface area, which is one of the

most important factors in achieving high catalyst performance, where the surface area of the porous material is one of the most significant parameters in determining its properties and the activity of the nanoparticles would be enhanced due to a high surface-to-volume ratio. The pore volume of nanomaterials produced with zeolite was enhanced, too. As a result, these sizes of pores provide more stability by acting as a covering agent to prevent the extreme reaction conditions of the nanoparticles' active sites, which are largely dependent on exposed pore channels due to their benefits for material diffusion. In this analysis, the pore size for GT-Z-Fe/Ni NPs was 11.54 nm and 12.76 nm for Z-Fe/Ni NPs which can be classified as mesopores according to the classification of the international union of pure and applied chemistry (IUPAC) that categorized the process of classification of the pore size as macropore (greater than 50 nm), mesopore (2 to 50 nm), super-micropore (0.7 to 2 nm), and ultra-micropore (smaller than 0.7 nm) [23]. Likewise, the results revealed that the pore size of zeolite 5A ranged from < 2- 50 nm which indicates that they have a high percentage of mesopore in the zeolite 5A.

**TABLE 2** The specific surface area (BET), pore-volume, average pore size, and Langmuir surface area of zeolite 5A and synthesis nanoparticles

Parameter	Zeolite -5A	GT-Z-Fe/Ni	Z-Fe/Ni
BET (m <sup>2</sup> /g)	221.10	18.47	32.72
pore volume (cm <sup>3</sup> /g)	0.15	0.05	0.10
Pore size (nm)	2.73	11.54	12.76
Langmuir surface area (m <sup>2</sup> /g)	316.80	910.71	1,484.69
Pore volume Single point.cm <sup>3</sup> /g	0.151	0.05	0.10
Pore volume B JH accumulation cm <sup>3</sup> /g	0.06	0.12	0.24
Adsorption average pore size diameter nm	2.73	11.54	12.54
Average pore size B JH nm	6.31	10.83	12.54

*Zeta potential analysis*

The Zeta potential measurement provides an important indicator for providing information about the stability of particles. The high zeta potential provides

nanoparticles with the stability they need to prevent aggregation, whereas the lower potential causes them to cluster together. This method is further used to determine the nanofluids' stability. Figure 6 displays the zeta potential value for the synthesis of

bimetallic (GT-Z-Fe/Ni and Z-Fe/Ni) nanoparticles by green and chemicals methods (-259.04 and -49.81) mV, respectively. The high negative zeta potential values of GT-Z-Fe/Ni NPS were attributed to the negative charge of green tea polyphenols. This result demonstrates the presence of polyphenols on the surface of nanoparticles. The electrostatic repulsive interactions between negatively charged nanoparticles

can prevent aggregation and hence improve stability. In terms of nanoparticle stability in environmental fluids, a zeta potential value of greater than 60 mV or less than -60 mV indicates excellent stability, a value of 40 to 60 mV or -60 to -40 mV signifies good stability, a value of 30 to 40 mV or -40 to -30 mV is stable, and a value ranging from -30 mV to 30 mV is highly agglomerative [24].

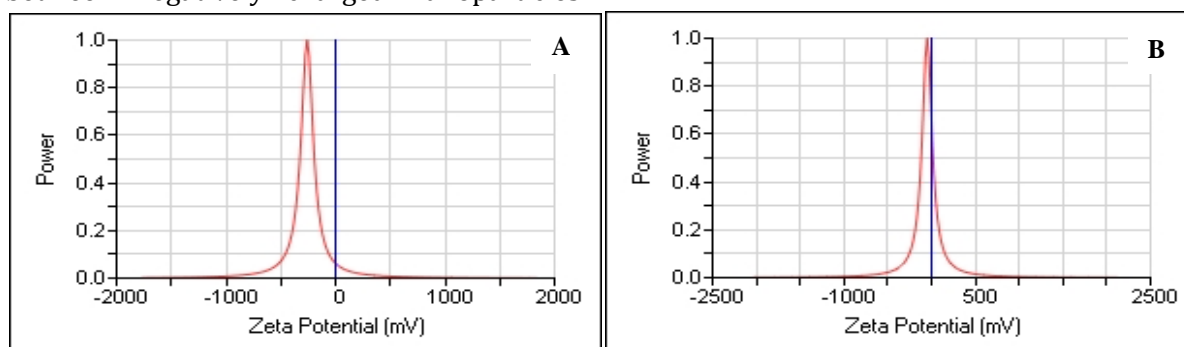


**FIGURE 6** Graphs of the zeta potential for synthesis nanoparticles A- [GT-Z-Fe/Ni] and B- [Z-Fe/Ni]

#### FT-IR spectroscopy

The Fourier-transform infrared spectroscopy (FT-IR) spectrum was recorded in the range of 400 to 4000  $\text{cm}^{-1}$  for bimetallic [GT-Z-Fe/Ni and Z-Fe/Ni] and zeolite, as depicted in Figure 7. It is used to investigate the functional groups attached to the surface of the nanoparticles. The FT-IR spectra of bimetallic [GT-Z-Fe/Ni] synthesized showed broadband stretching vibrations of strong group O-H observed in the band (3392.79)  $\text{cm}^{-1}$ , this belongs to polyphenol compounds as shown in Figure 7A. Polyphenols can be assumed as reducing and capping agents. This indicates the presence of polyphenol compounds in the synthesis of bimetallic GT-Z-Fe/Ni NPs [21]. In bimetallic Z-Fe/Ni NPs, a broadband stretching vibration of strong group OH was observed at 3402.43  $\text{cm}^{-1}$ , as well as a band of an O-H bending vibration of Z-Fe/Ni at 1637.56  $\text{cm}^{-1}$ , which may belong to the ethanol that keeps the NPs in Figure 7 (B). The absorption bands at 2900.94  $\text{cm}^{-1}$  of the C-H group and the bands at 1631.78  $\text{cm}^{-1}$  reveal the presence of a C=O stretching

vibration of polyphenols; the bands at 1581.63  $\text{cm}^{-1}$  of C=C aromatic ring stretching and the band at 1429.25  $\text{cm}^{-1}$  of C-H aromatic stretching; the bands of 1346.31-1215.15  $\text{cm}^{-1}$  belong to O-H stretching and 1070.49  $\text{cm}^{-1}$  denote the existence of a C-O-C symmetric stretching vibration of polyphenols presence in GT-Z-Fe/Ni [25]. The bands described above belonged to the characteristic peaks of green tea extracts. This indicates that the effective components in green tea extracts can be coated onto the surface of [GT-Z-Fe/Ni] particles. Figure 7A demonstrates that the presence and intensity of phenolic compound peaks can reduce Fe, and are a strong indicator of synthesized GT-Z-Fe/Ni [6]. A small absorption band at 1006.86  $\text{cm}^{-1}$  for C-O-C and a small absorption band at 470.36  $\text{cm}^{-1}$  for Fe-O in Z-Fe/Ni NPs. This indicates that a small portion of the NZVI particles was oxidized in Z-Fe/Ni synthesis chemically compared with G-Z-Fe/Ni synthesis by the green methods. It was most likely caused by a coordination reaction between the oxygen atom's lone pair of electrons and the iron atom's 3d space

orbital, which resulted in a decrease in the O-H group's electron cloud density and the bond force constant, weakening the O-H stretching vibration bond [22]. The new bands appeared in GT-Z-Fe/Ni and Z-Fe/Ni at (1029.99 and 1008.77  $\text{cm}^{-1}$ ) and (1006.84  $\text{cm}^{-1}$ ), respectively, this may be attributed to the bending vibration of Si-O vibrations, as illustrated in Figure 7A and B. The absorption peak near 759.95  $\text{cm}^{-1}$  was caused by the antisymmetric stretching vibration of Si-O-Si in the zeolite of [GT-Z-Fe/Ni]. The bands at 578.64  $\text{cm}^{-1}$ , 534.28  $\text{cm}^{-1}$ , and 542.00  $\text{cm}^{-1}$  indicate the presence of bending vibrations of Si-O-Al and Si-O-Si in GT-Z-Fe/Ni, Z-Fe/Ni,

and zeolite, respectively. No new bands at  $<900 \text{ cm}^{-1}$  were observed with (GT-Z-Fe/Ni and Z-Fe/Ni) NPs indicating the slight oxidation of NZVI on the surface of zeolite [15]. In Figure 7C, the characteristic peaks at (3437.15 and 1647.21)  $\text{cm}^{-1}$  were attributed to the stretching and bending vibration of OH, respectively and the band at 1029.99  $\text{cm}^{-1}$  corresponded to the Si-O-Si anti-symmetric stretching vibration. The band around 1006.84  $\text{cm}^{-1}$  can be attributed to the stretching vibration of Si-O. The bands observed at 688.59, 542.00  $\text{cm}^{-1}$  were due to quarts or amorphous  $\text{SiO}_2$  stretching vibration and Si-O-Al bending mode [15].

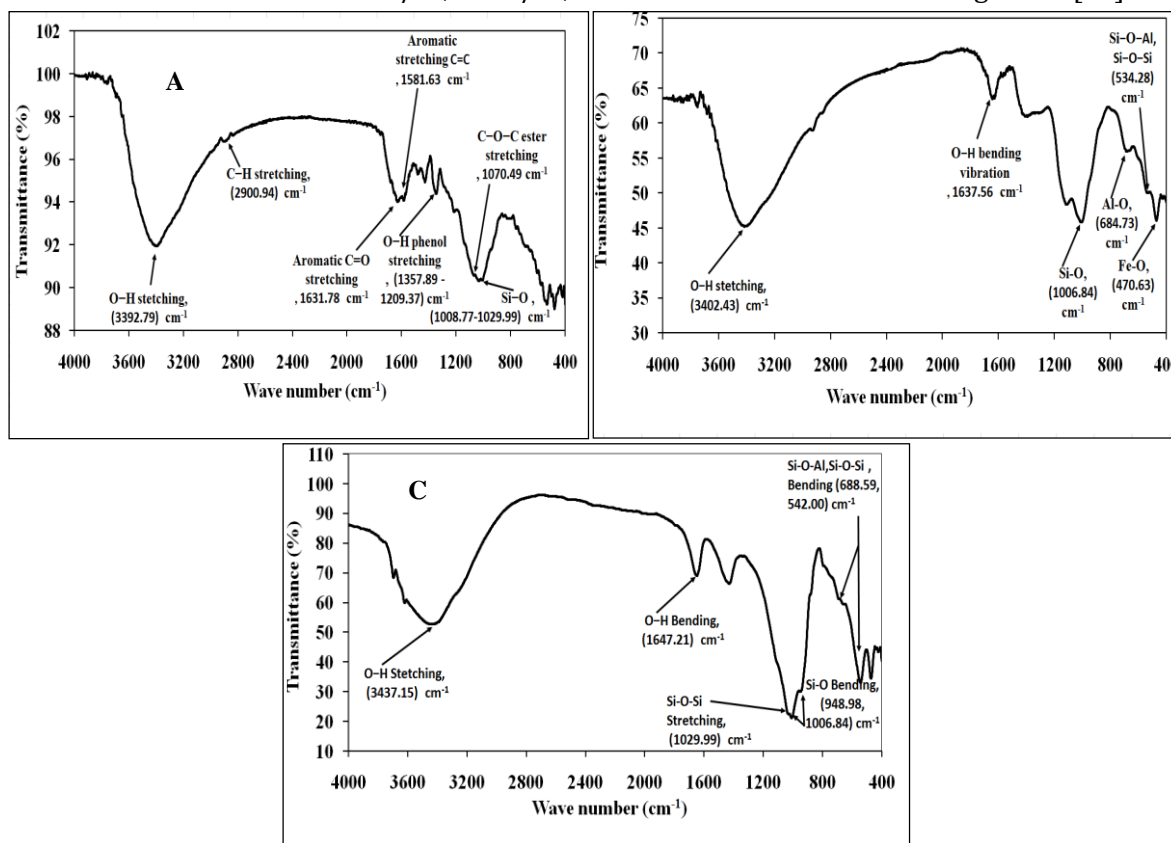


**FIGURE 7** FT-IR Spectroscopy of (A): GT-Z-Fe/Ni and (B): Z-Fe/Ni(C): Zeolite 5A

*The optimum conditions for the removal of RR120 dye*

The removal of RR120 dye from aqueous solutions by GT-Z-Fe/Ni and Z-Fe/Ni in a heterogeneous Fenton-like oxidation experiments was carried out in an open system, and the removal efficiency was

evaluated and determined under various experimental conditions, such as  $\text{H}_2\text{O}_2$  concentrations, doses of NPs, initial pH, initial RR120 dye concentrations, and the effect of temperature, which were used to determine the RR120 dye removal efficiency performance by using Equation 3 and

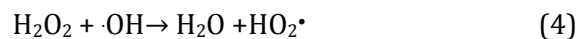


determine the optimum conditions for removal.

#### The concentration effects of hydrogen peroxide

The concentration of hydrogen peroxide is a very important parameter for the maximum decolorization efficiency of RR120 dye from aqueous solutions. In general, the removal efficiency of RR120 increases as the hydrogen peroxide concentration increases until it reaches a critical concentration, at which point it decreases in which the amount of dye removed reduces [7]. The effects of different concentrations of  $H_2O_2$  (0.1-7.5) and (0.1-20) mmol/L in the state of GT-Z-Fe/Ni and Z-Fe/Ni NP, respectively in Fenton-like experiments on the removal of RR120 dye aqueous solution at the experiment conditions (NPs (0.1 and 0.5) g/L, dye aqueous solution 25 mg/L, and initial pH=3 at room temperature. The decolorization efficiency of catalyzed zeolite supported on (Fe/Ni) NPs synthesized by green methods (GT-Z-Fe/Ni) increased from (83.5 to 99.09%) after 120 minutes of heterogeneous Fenton oxidation when the hydrogen peroxide concentration was increased from 0.1 to 7.5 mmol/L and decreased with increasing the hydrogen peroxide concentration (up to 7.5 mmol/L), as depicted in Figure 8 (A). The decolorization efficiency for RR120 dye increased as the hydrogen peroxide concentration was

increased because it produced a large formation of  $\cdot OH$  free radical when the amount of  $H_2O_2$  was increased. The reason for this decrease could be that the  $\cdot OH$  free radical was gradually consumed from the solution and replaced with less reactive  $HO_2\cdot$  as explained in Equations 4, [6].



While (Z-Fe/Ni) syntheses by chemical methods, the decolorization efficiency increased with enhancing hydrogen peroxide concentration from 0.1 to 20 mmol/L from (88.5 to 91.6%) at 120 min heterogeneous Fenton oxidation, as indicated in Figure 8B. According to the results, the reaction rate is very fast during heterogeneous Fenton oxidation from (5–120) min. Therefore, in the state of catalyzed Z-Fe/Ni, the reaction rate is extremely fast from (2-120) min. The optimum concentration of  $H_2O_2$  for the removal of RR120 dye aqueous solution (1 mmol/L) and (7.5 mmol/L) by the GT-Z-Fe/Ni and Z-Fe/Ni NPs, respectively. When Fe/Ni particles were loaded onto zeolite, they had a much higher surface area, pore-volume, and pore reduced size, indicating that the supported zeolite played an important role in dispersing Fe/Ni and thus increasing surface area and active sites for reactivity improvement, a large formation of  $\cdot OH$  free radical in low amounts of  $H_2O_2$ , and nanoparticles.

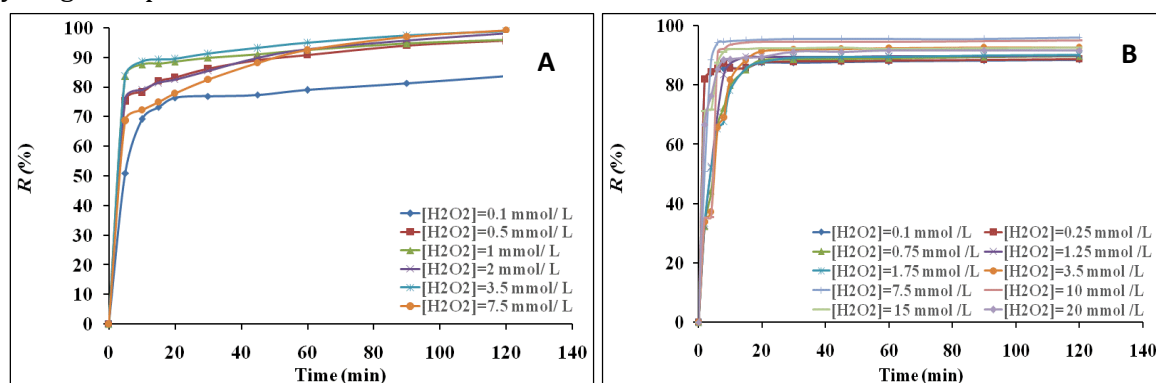


**FIGURE 8** Decolorization efficiencies of RR120 dye with various concentrations of  $H_2O_2$ (A): GT-Z-Fe/Ni and (B): Z-Fe/Ni

### The amount effects of nanoparticles on dye removal

The effects of bimetallic GT-Z-Fe/Ni and Z-Fe/Ni nanoparticle doses in the range of (0.05-1.5) g/L were examined in Fenton-like experiments using the optimal concentration of H<sub>2</sub>O<sub>2</sub> (1 and 7.5) mmol/L, respectively on the degradation of a solution prepared of (25 mg/L) RR120 dye at a pH of 3, as displayed in Figure 9. The decolorization efficiency of catalyzed GT-Z-Fe/Ni decreased from 99.8% to 58.6% after 120 minutes when the GT-Z-Fe/Ni nanoparticle dose was increased from 0.1 to 1.5 g/L and decreased when the dose was less than 0.1 g/L. From (5–120) min, the reaction rate is extremely fast, and the optimum NPs doses are obtained at 0.1 g/L[26]. While the decolorization efficiency increases with nanoparticle dose increase from 68.8 to 99.8 in the state of (Z-Fe/Ni) at 120 min heterogeneous Fenton oxidation, the reaction is very fast and the RR120 dye is removed in a short time. Based on the results, it is concluded that the elimination effectiveness of RR120 dye solutions was lower at higher doses of GT-Z-Fe/Ni NPs and higher at higher doses of Z-Fe/Ni NPs, as illustrated in Figure 9. This is due to the presence of green tea (polyphenols) on the

surface of the GT-Z-Fe/Ni nanoparticles. More polyphenols are discharged into the aqueous dye solution and consumption ·OH free radical may result from increasing the amount of GT-Z-Fe/Ni NPs(6), and the decolorization efficiency is significantly improved. The green methods are simple, economical, inexpensive, non-toxic, and environmentally friendly processes for the synthesis of nanoparticles and an environmentally friendly approach that avoids the use of harmful chemicals because of its low cost and great efficiency for industrial large-scale production. The zeolite supported enhanced the reactivity of Fe/Ni NPs nanoparticles because the surface area and active sites were increased, resulting in the large formation of ·OH free radical in a low amount of H<sub>2</sub>O<sub>2</sub> and nanoparticles. Fe/Ni nanoparticles dispersed uniformly on the surface could reduce the size of Fe/Ni nanoparticles and make them dispersed uniformly on the surface, which may accelerate the reactivity of Fe/Ni nanoparticles and improve RR120 dye removal by generating more Fe<sup>2+</sup> and Fe<sup>3+</sup>, as well as metal oxides and hydroxides, increasing dye removal through a complex action or co-precipitation [15].

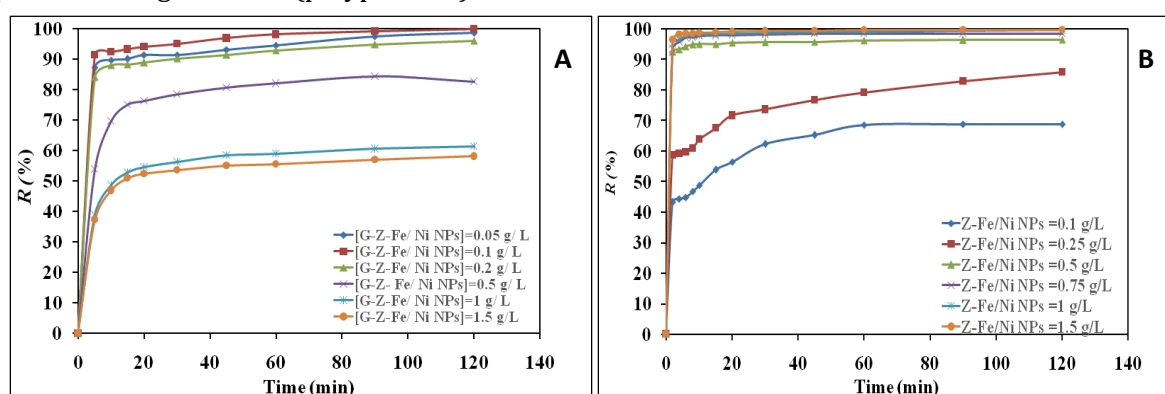


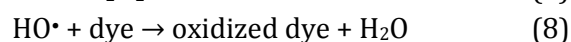
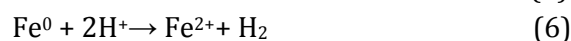
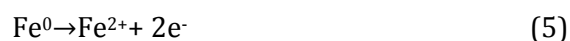
**FIGURE 9** Decolorization efficiencies of RR120 dye with various dosages of (A): GT-Z-Fe/Ni and (B): Z-Fe/Ni

### The pH effect of solution

The removal of organic pollutants from aqueous media by the Fenton-like process is greatly influenced by pH value because of its

effects on catalyst performance and H<sub>2</sub>O<sub>2</sub> stability, as well as the production of highly reactive substances ·OH free radical. Under the following experimental conditions, the effect of pH was evaluated for (2.5- 9) to get

the optimum pH for dye degradation, [RR120 dye] = 25 at the optimum concentrations of [H<sub>2</sub>O<sub>2</sub>] = (1 and 7.5) and dosages for bimetallic [GT-Z-Fe/Ni] and [Z-Fe/Ni] NPS (0.1 and 0.5) g/L, respectively, at room temperature. After 120 min of Fenton-like oxidation reactions catalyzed by bimetallic [GT-Z-Fe/Ni and Z-Fe/Ni] nanoparticles, the RR120 dye removal efficiency at various pH was (100, 99.8, 17.6, 10, 9.8, and 5) and (96.6, 96.6, 94, 92.7, 92, and 83.9%), respectively. From the results for bimetallic [GT-Z-Fe/Ni and Z-Fe/Ni], then the nanoparticles indicated that there was an increase in the decolorization efficiency of RR120 dye with a decrease in aqueous pH and a decrease in the decolorization efficiency of RR120 dye with an increase in pH aqueous solution, with the best removal performance of the RR120 dye occurring at pH 2.5 and 3, with decolorization efficiencies of 100 and 99.8% and 96.6 and 96.6% in RR120 dye, respectively. When bimetallic [GT-Z-Fe/Ni] and [Z-Fe/Ni] are oxidized in solutions with low pH values, ferrous hydroxide clogs the nano iron surface, resulting in this behavior [26]. The reason for this behavior is related to a Fenton-like mechanism and the production of •OH free radical. At low pH values, the reaction between Fe<sup>0</sup> in Fe/Ni NPs and H<sub>2</sub>O<sub>2</sub> is accelerated at low pH values to produce Fe<sup>+2</sup>. These ions surround the surface and react with H<sub>2</sub>O<sub>2</sub> to generate •OH free radical, as illustrated in the following Equations (5-9), [27].



Furthermore, the high acidic medium at pH levels below 2.5 resulted in an excess of H<sup>+</sup> ions, which contributed to a decrease in the number of highly reactive •OH free radical and, as a result, a decrease in removal efficiency. The decrease in •OH free radical

results in the inability to convert Fe<sup>+3</sup> into Fe<sup>+2</sup> efficiently. Additionally, because ferrous ions and hydrogen peroxide are unstable at higher pH values (values above 4), the catalyst would precipitate and form complex by-products (ferric hydroxo complexes), causing the H<sub>2</sub>O<sub>2</sub> to decompose and lowering the removal effectiveness (6). At these higher pH values, the elimination of RR120 dye was completed by coagulation or sorption instead of oxidation. The influence of a solution's initial pH on RR120 dye adsorption by bimetallic [GT-Z-Fe/Ni and Z-Fe/Ni] nanoparticles was illustrated in Figures 10A and B. According to the research results, higher RR120 dye adsorption could be due to two causes: (1) At pH=3, the H<sup>+</sup> concentration in the solution was extremely high, increasing the electrostatic attraction between the H<sup>+</sup> solution and the adsorbent, [23]. The degree of ionization, the surface load of the sorbent, and the adsorbate classes can be influenced by pH. This could be attributed to the reason that at low pH, the Fe/Ni NPs surface has a positive charge, whereas dye molecules with a sulfonic group (SO<sub>3</sub>) have a negative charge, attracting the NZVI particles. They discovered that decolorization significantly improved the pH of acidic solutions. The reaction rate of the RR120 dye removal in the state of GT-Z-Fe/Ni nanoparticles is extremely rapid (5 to 120) min and this catalyst only operates in an acidic medium and not with a pH greater than 3, as displayed in Figure 10A. While in the state of Z-Fe/Ni nanoparticles, the reaction is very fast, removing the RR120 dye in 2 to 120 min. It works well in acidic media, neutral and basic solutions, but not in solutions with a pH greater than 9, and the best pH values are 2.5 and 3, as demonstrated in Figure 10B. Both catalysts do not work in (pH less than 2.5), and when the original solution pH was lower, more H<sup>+</sup> was consumed during RR120 removal. H<sup>+</sup> could prevent the formation of the oxide layer on the surface of NPs, revealing more active sites and increasing the removal rate [15].

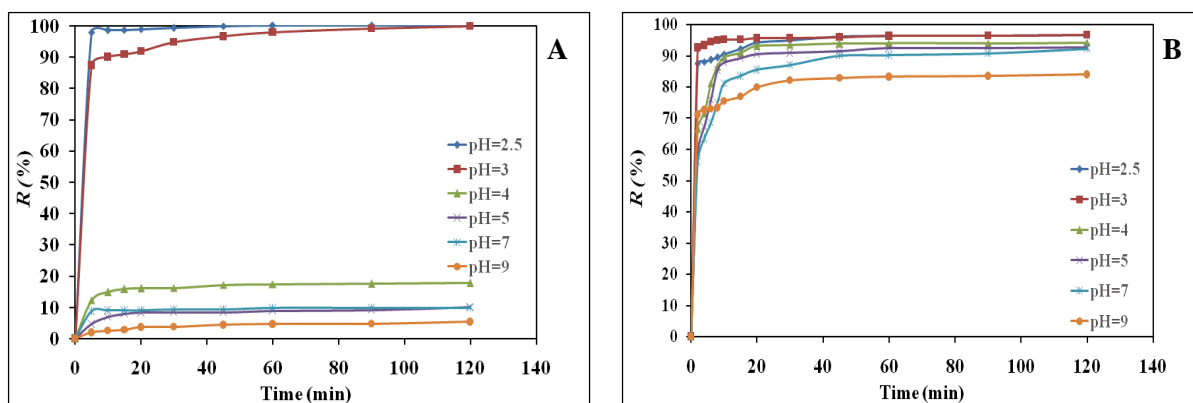


**FIGURE 10** Decolorization efficiencies of RR120 dye in solutions at various pH levels for (A): GT-Z-Fe/Ni and (B): Z-Fe/Ni

#### The Effect of initial dye concentration

The initial dye concentration is a function of the removal rate, making it an important parameter to consider for effective adsorption. Additionally, the initial dye concentration provides a driving force able to overcome the resistance of dye ions' transfer between the liquid and solid phases. The initial concentrations of RR120 dyes were studied in the range of (15, 20, 25, 50, 75, and 100) mg/L at the optimum conditions of  $[H_2O_2] = (1 \text{ and } 7.5) \text{ mmol/L}$  for GT-Z-Fe/Ni and Z-Fe/Ni NPs, bimetallic GT-Z-Fe/Ni and Z-Fe/Ni NPs dosages of (0.1 and 0.5) g/L, pH = 3 and at room temperature within (0–120) min. Figure 11 displays the effect of RR120 dye concentration on the removal efficiency of the RR120 dye, which was a decrease from

(100 – 26.7%) and (98 – 61%)% for bimetallic GT-Z-Fe/Ni and Z-Fe/Ni NPs, respectively, within 120 min of the reaction time. Figure 11 demonstrates that the removal of RR120 dye decreases as the dye concentration increases, the quantity of reactive  $\cdot OH$  free radical in the medium clearly limits degradation performance, with larger concentrations requiring more hydroxyl radicals. Furthermore, by-products of the Fenton-like reaction may have tried to compete with dye molecules for catalytic active sites, resulting in a slower degradation rate. A decrease in dye concentration results in an increase in dye decolorization effectiveness due to the small dye particles available for purification by the hydroxyl radicals (26).

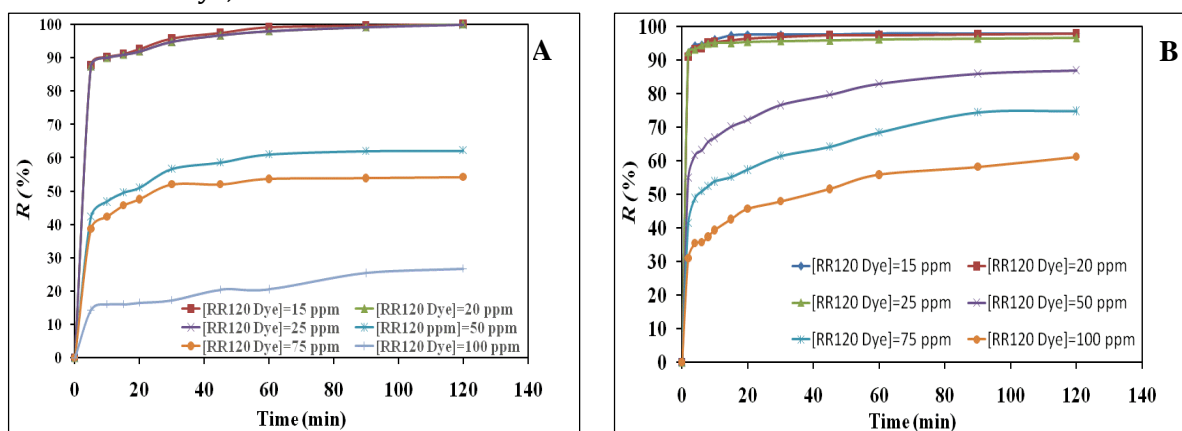


**FIGURE 11** Decolorization efficiencies of RR120 dye concentration at optimum conditions for (A): GT-Z-Fe/Ni and (B): Z-Fe/Ni

### Effect of temperature

The effect of Fenton-like oxidation reactions on the removal efficiency of RR120 dye (100 mg/L) was studied at temperatures ranging from (30 to 50) °C. The tests were carried out to examine the removal of dye at the optimum conditions of  $[H_2O_2] = (1 \text{ and } 7.5) \text{ mmol/L}$ , bimetallic nanoparticle dosages of (0.1 and 0.5) g/L for [GT-Z-Fe/Ni] and [Z-Fe/Ni] NPs, respectively and pH=3. The decolorization efficiency of the processes catalyzed by GT-Z-Fe/Ni and Z-Fe/Ni NPS increased from (26.7 to 97.4 and 99.8) and (61 to 70 and 90%), respectively, when the temperature was raised from 30-50 °C. The

best temperature for the degradation of RR120 dye is between (40-50) °C for bimetallic GT-Z-Fe/Ni nanoparticles and (50) °C for Z-Fe/Ni nanoparticles. The removal percentage increased as the temperature increased from (30 to 50) °C [26]. This could be because greater temperatures tend to increase the oxidation reaction rate between the catalyst and  $H_2O_2$ , leading to an increase in the production rate of  $\cdot OH$  free radical or high valence iron species. High temperatures can provide more energy to reactant molecules, allowing them to overcome the energy required for reaction activation [6,26,28].

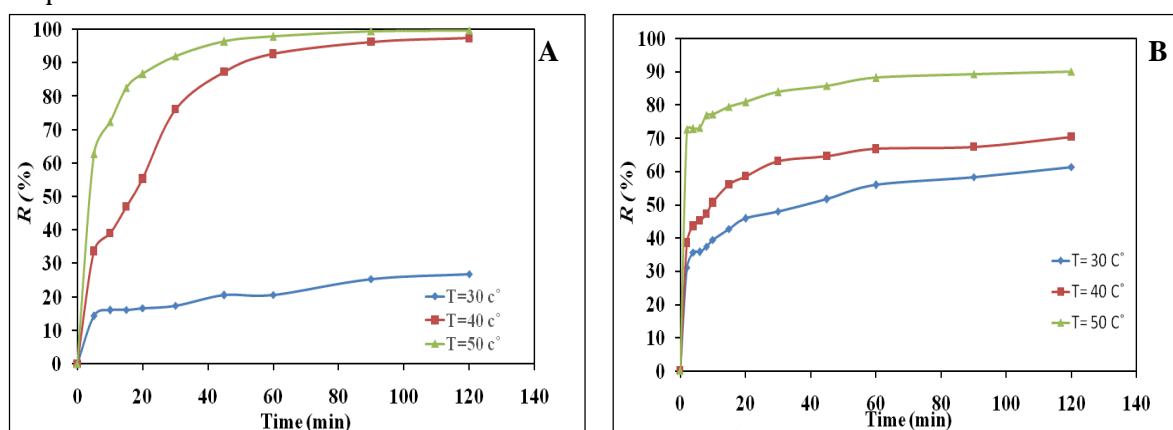


**FIGURE 12** Decolorization efficiencies of RR120 dye in solutions at various temperatures. (A): GT-Z-Fe/Ni and (B): Z-Fe/Ni

### Kinetics of RR120 dye removal by fenton-like process

Three kinetic models for RR120 dye decolorization kinetic rates by the Fenton-like oxidation reaction were used to calculate the decolorization rate constants using the linear forms of the first-order, the second-order [5,29], and Behnajady-Modirshahla-Ghanbary (BMG) models [20,23], as shown in Equations 10-12, respectively. The value of the rate constant  $k_1$  for first-order ( $\text{min}^{-1}$ ) was calculated from the slope of the graph between  $\ln C_0/C_t$  and time ( $t$ ) according to Equation 10. Besides, the values of  $k_2$  for second-order ( $\text{L}/(\text{mol} \cdot \text{min})$ ) were obtained from the slope of the plot between  $1/C_t$  and  $t$

according to Equation 11. The concentration of the RR120 dye ( $C_0$  and  $C_t$ ) at times 0 and  $t$ , respectively.

$$\ln C_0/C_t = K_1 t \quad \text{First - order} \quad (10)$$

$$1/C_t - 1/C_0 = K_2 t \quad \text{Second-order} \quad (11)$$

$$t/[1 - (C_t/C_0)] = m + b t \quad \text{BMG models} \quad (12)$$

The rate constant  $K_1$  increases with the increase of  $H_2O_2$  concentration, the dosage of NPs, and temperature and decreases with the increase of initial RR120 dye concentration and pH. Tables 3 and 4 show the parameters of the model for bimetallic GT-Z-Fe/Ni and Z-Fe/Ni NPs with the corresponding correlation coefficient for each factor. From the result, the first order was not fitted for degradation of RR120 dye by the Fenton-like oxidation



reaction due to having low values for the regression coefficient  $R^2$  compared with other kinetic models for each NPs. In bimetallic GT-Z-Fe/Ni, the decolorization kinetic rate constant  $K_2$  of RR120 dye catalyzed by the Fenton-like oxidation reaction increased with increasing  $H_2O_2$  and temperature because of the thermal decomposition of  $H_2O_2$ , the rate of degradation was increased at a temperature higher than 313 K and decreased with increasing (the dosage of GT-Z-Fe/Ni NPs, pH, and the concentration of RR120 dye) increases. Based on the results, it is evident that the linear fitting value of the regression coefficient  $R^2$  for the second-order is higher than  $R^2$  for first-order, which indicates that the second-order kinetic model is well fitted for RR120 dye kinetic degradation by a Fenton-like process catalyzed by GT-Z-Fe/Ni-NPs [7]. The second-order model fits the degradation of the RR120 dye by the Fenton-like reaction by using bimetallic nanoparticles (Z-Fe/Ni) synthesis by chemical methods, as well. The Behnajady-Modirshahla-Ghanbary (BMG) kinetic model for RR120 dye decolorization kinetic rates by the Fenton-like oxidation reaction at different conditions was calculated from a line of  $t/[1-(C_t/C_0)]$  vs.  $t$  values in a straight line with a slope  $m$  (min) and an intercept  $b$  in the BMG model Equation 12. In the Fenton-like oxidation

process by GT-Z-Fe/Ni NPs, show decrease or increase in the values of  $m$ , but the values of  $b$  decrease with increasing the concentration of  $H_2O_2$  and with increasing the dosage of nanoparticles, as well as the  $m$  and  $b$  values increased at various pH. As the initial concentration of RR120 dye increased, the values of  $m$  and  $b$  increased. A Fenton-like process was used at a different temperature that reduced the parameters  $m$  and  $b$ . The BMG kinetic model has a higher correlation coefficient  $R^2$  value than the other models indicating that it fits the experimental data better, as observed in Table 3. In the Fenton-like oxidation process by Z-Fe/Ni NPs, the values of  $m$  increased with the concentration of  $H_2O_2$  increasing from 0.1 to 10 mmol/L and began to gradually decrease after the concentration of  $H_2O_2$  increased from 15 to 20 mmol/L. The values of the  $b$  parameter decrease with an increase in the concentration of  $H_2O_2$  from 0.1 to 20 mmol/L, the  $m$  and  $b$  values increased at different pH, as well as, with the concentration of RR120 dye increased, the values of  $m$  and  $b$  increased. While the  $m$  and  $b$  values decreased as the temperature rose from 30 to 50 °C. Furthermore, depending on the RR120 removal regression coefficient values, the BMG kinetic model has a higher correlation coefficient  $R^2$  value than other models and fits the experimental data, as indicated in Table 4.

**TABLE 3** The first-order, the Second-order, and BMG Kinetics parameters for the Fenton-like reaction of RR120 for the studied parameters by GT-Z-Fe/Ni NPs

Parameters		RE % After 15 min	RE % After 120 min	First- Order		Second-Order		BMG		
				$K_1$ ( $\text{min}^{-1}$ )	$R^2$	$K_2$ L/(mol. min)	$R^2$	$m$ (min)	$B$	$R^2$
Initial $H_2O_2$ Concentration (mmol / L)	0.1	73.23	83.75	0.011	0.526	0.001	0.737	2.923	1.193	0.998
	0.5	81.91	95.57	0.018	0.743	0.006	0.982	2.476	1.039	0.999
	1	87.88	95.89	0.016	0.573	0.006	0.947	1.455	1.043	0.999
	2	81.35	98.15	0.025	0.868	0.014	0.862	2.901	1.011	0.998
	3.5	89.27	98.72	0.025	0.777	0.020	0.870	1.647	1.010	0.999
	7.5	74.96	99.09	0.032	0.954	0.027	0.747	4.301	0.991	0.996
Average $R^2$					0.740		0.857			0.998
GT-Z-Fe/Ni NPs Doses (g/L)	0.05	89.94	98.51	0.023	0.710	0.018	0.896	1.674	1.007	0.999
	0.1	93.14	99.90	0.037	0.842	0.132	0.680	0.995	0.998	0.999
	0.25	88.18	96.00	0.030	0.921	0.008	0.793	1.455	1.043	0.999
	0.5	74.99f	82.60	0.009	0.492	0.001	0.672	4.475	1.059	0.980
	1	52.66	61.41	0.004	0.444	0	0.559	3.977	1.608	0.999

Average R <sup>2</sup>	1.5	50.81	58.03	0.004	0.41	0	0.502	3.901	1.709	0.999
					0.637		0.684			0.996
	2.5	98.67	100	0.033	0.527	0.189	0.956	0.093	1.002	1
Initial pH	3	90.00	99.90	0.039	0.884	0.133	0.684	1.205	0.996	0.999
	4	15.77	17.68	0	0.318	4×10 <sup>-5</sup>	0.334	10.91	5.590	0.999
	5	7.82	10.11	0	0.470	2×10 <sup>-5</sup>	0.482	50.09	9.961	0.992
	7	8.93	9.88	0	0.228	2×10 <sup>-5</sup>	0.234	14.00	10.01	0.999
	9	2.85	5.32	0	0.688	1×10 <sup>-5</sup>	0.695	185.0 0	18.17	0.986
Average R <sup>2</sup>					0.519		0.557			0.996
Initial RR120 Dye Concentration (mg/L)	15	91.02	100	0.038	0.815	0.101	0.930	1.062	0.994	0.999
	20	90.00	100	0.036	0.883	0.077	0.870	1.554	0.994	0.999
	25	90.94	99.90	0.035	0.854	0.074	0.835	1.205	0.996	0.999
	50	49.62	62.14	0.005	0.515	0	0.646	0.824	2.003	0.995
	75	45.69	54.18	0.003	0.409	9×10 <sup>-5</sup>	0.498	3.917	1.814	0.999
Average R <sup>2</sup>	10	16.05	26.76	0.001	0.706	2×10 <sup>-5</sup>	0.757	35.55 0	3.658	0.973
					0.697		0.756			0.994
	30	16.05	26.76	0.001	0.706	2×10 <sup>-5</sup>	0.757	35.55 0	3.658	0.973
Temperature (°C)	40	47.05	97.42	0.032	0.955	0.003	0.957	0.780	0.780	0.871
	50	82.52	99.81	0.048	0.969	0.036	0.766	2.751	0.982	0.999
Average R <sup>2</sup>					0.877		0.827			0.948

**TABLE 4** The first-order, the Second-order, and BMG Kinetics parameters for the Fenton-like reaction of RR120 for the studied parameters by Z-Fe/Ni NPs

Parameter	RE % After 15 min	RE % After 120 min	First- Order		Second-Order		BMG			
			$K_1$ (min <sup>-1</sup> )	R <sup>2</sup>	$K_2$ L/(mol.min)	R <sup>2</sup>	$M$ (min)	$b$	R <sup>2</sup>	
Initial H <sub>2</sub> O <sub>2</sub> Concentration (mmol/L)	0.1	85.74	88.51	0.006	0.177	0.001	0.348	0.302	1.128	1
	0.25	85.74	88.88	0.006	0.173	0.001	0.336	0.296	1.124	1
	0.75	85.87	89.77	0.002	0.440	0.002	0.594	2.015	1.092	0.999
	1.25	89.59	89.96	0.012	0.332	0.002	0.410	1.308	1.096	0.999
	1.75	85.66	90.31	0.015	0.496	0.003	0.633	2.016	1.086	0.999
	3.5	88.45	92.73	0.018	0.489	0.004	0.615	2.2.325	1.051	0.998
	7.5	95.14	96.07	0.013	0.227	0.005	0.368	0.386	1.039	0.999
	10	94.39	95.11	0.006	0.794	0.004	0.401	1.691	1.036	0.996
	15	92.07	92.64	0.010	0.237	0.002	0.315	0.334	1.076	0.999
	20	89.22	91.68	0.010	0.307	0.002	0.492	0.476	1.085	1
Average R <sup>2</sup>				0.367		0.387				0.998
Z-Fe/Ni NPs Doses (g/L)	0.1	53.91	68.84	0.006	0.614	0	0.749	4.399	1.414	0.998
	0.25	67.59	85.92	0.011	0.710	0.001	0.938	3.494	1.162	0.997
	0.5	95.16	96.65	0.010	0.208	0.005	0.557	0.178	1.034	1
	0.75	97.95	98.51	0.014	0.234	0.016	0.546	0.206	1.005	0.999
	1	98.33	99.63	0.024	0.455	0.073	0.957	0.165	1.003	1
	1.5	99.05	99.81	0.030	0.481	0.199	0.891	0.086	1.001	1
Average R <sup>2</sup>				0.540		0.773				0.999
Initial pH	2.5	92.17	96.64	0.016	0.454	0.008	0.810	0.509	1.031	1
	3	95.16	96.65	0.010	0.208	0.005	0.557	0.178	1.034	1
	4	90.87	94.22	0.015	0.415	0.004	0.606	0.689	1.054	0.999
	5	89.19	92.73	0.014	0.428	0.003	0.643	0.922	1.070	0.999
	7	83.42	92.17	0.015	0.587	0.003	0.833	1.683	1.077	0.999
	9	76.88	83.98	0.007	0.354	0.001	0.588	1.002	1.185	0.999
Average R <sup>2</sup>				0.416		0.672				0.999
Initial RR120 Dye Concentration	15	97.40	98.04	0.014	0.273	0.019	0.577	0.147	1.021	1
	20	96.00	97.88	0.015	0.336	0.019	0.754	0.235	1.020	1
	25	95.16	96.65	0.010	0.208	0.005	0.557	0.178	1.034	1

(mg/L)	50	70.27	86.96	0.012	0.704	0.001	0.930	3057	1.37	0.998
	75	55.28	74.90	0.008	0.708	0	0.887	5.218	1.317	0.995
	100	42.65	61.31	0.005	0.712	0	0.841	7.993	1.617	0.994
Average R <sup>2</sup>					0.490		0.757			0.997
Temperature	30	42.65	61.31	0.005	0.712	0	0.841	7.993	1.161	0.994
(°C)	40	42.80	70.38	0.007	0.599	0	0.756	4.108	1.393	0.998
	50	79.40	90.03	0.011	0.558	0	0.872	1.624	1.104	0.999
Average R <sup>2</sup>					0.623		0.823			0.997

### Thermodynamic of dye removal by Fenton-like process

The thermodynamic parameters of enthalpy ( $\Delta H^\circ$ ), entropy ( $\Delta S^\circ$ ), and Gibbs free energy ( $\Delta G^\circ$ ) were calculated [2,5,20] using Equations 13 to 15 depending on the removal of RR120 dye by Fenton-like oxidation reaction using (GT-Z-Fe/Ni and Z-Fe/Ni) NPs at 303, 313, and 323 K, as listed in Table 5.

$$K_d = (C_0 - C_e) / C_e \times (v/m) \quad (13)$$

$$\Delta G^\circ = -RT \ln K_d = \Delta H^\circ - T \Delta S^\circ \quad (14)$$

$$\ln K_d = (\Delta S^\circ) / R - (\Delta H^\circ) / RT \quad (15)$$

From Equation 15 a straight-line graph of  $\ln K_d$  vs.  $1/T$  values with a slope equal to  $(-$

$\Delta H^\circ) / R$  and an intercept equal to  $\Delta S^\circ / R$ , where  $R$  is the ideal gas constant (8.314 J/mol. K). Figure 13 reveals the linear plots of thermodynamic data calculated for GT-Z-Fe/Ni NPs and Z-Fe/Ni NPs at various temperatures. Table 5 demonstrates that the Gibbs free energy  $\Delta G^\circ$  is negative, indicating spontaneous reaction nature [30] and the positive values for  $\Delta H^\circ$  and  $\Delta S^\circ$  illustrate the removal of the RR120 dye by Fenton-like oxidation using (GT-Z-Fe/Ni and Z-Fe/Ni) NPs were endothermic processes [20,30] and random reactions.

**TABLE 5** The calculated values of the thermodynamic factors of RR120 dye in Fenton-like oxidation reactions by using various NPs after 120 minutes at various temperatures

NPs	T (K)	$\Delta G^\circ$ K.J/mol	$\Delta H^\circ$ K.J/mol. K	$\Delta S^\circ$ K.J/mol. K
GT-Fe/Ni	303.15	-2.389239616	210.82641	0.70660686
	313.15	-12.59245393		
	323.15	-16.38542659		
Z-Fe/Ni	303.15	-2.342649251	71.533656	0.24260252
	313.15	-3.747002571		
	323.15	-7.239858992		

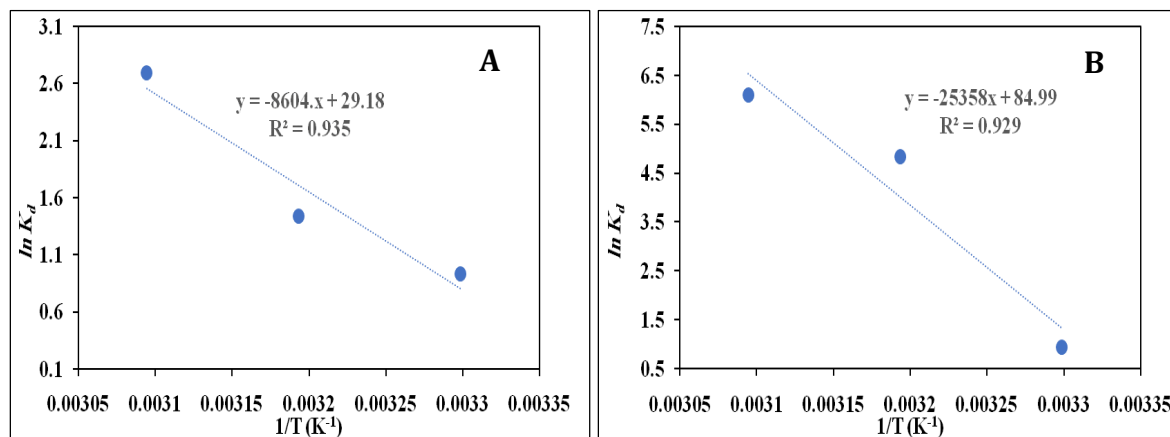


**FIGURE 13** Linear plots of thermodynamic data calculated for (A)- GT-Z-Fe/Ni NPs and (B)- Z-Fe/Ni NPs at various temperatures

### Comparison of decolorization efficiency by using different reaction mechanisms

The efficiency of decolorization employing various reaction processes is compared as indicated in Figure 14. At the optimum conditions, the efficiency of RR120 dye removal in an aqueous solution was examined as heterogeneous Fenton-like oxidation reaction and adsorbent catalyst by various catalysts, such as (GT-Z-Fe/Ni), (Z-Fe/Ni), and zeolite 5A. The decolorization efficiency of RR120 dye by Fenton-like oxidation processes and adsorbent processes without using  $H_2O_2$  by GT-Z-Fe/Ni NPs was 99.90% and 6.30%, respectively, at room temperature. In contrast, the decolorization efficiency of RR120 dye by Fenton-like oxidation processes and adsorbent processes using GT-Z-Fe/Ni NPs was 96.65 and 91.26%, respectively, at room temperature, as reported in Table 6. At optimum conditions, the decolorization efficiency of RR120 dye by zeolite 5A was studied as an adsorbent catalyst and was (28%). The difference in removal efficiency indicates that the reactivity of bimetallic GT-Z-Fe/Ni and Z-Fe/Ni with and without  $H_2O_2$  varied significantly. This is usually due to their morphology and reaction mechanisms. The removal efficiency of RR120 dye utilizing GT-Z-Fe/Ni and Z-Fe/Ni with the Fenton-like oxidation reaction was higher than the

removal efficiency by adsorption processes without using  $H_2O_2$ . Furthermore, the removal efficiency of Z-Fe/Ni NPs by adsorption processes was greater than GT-Z-Fe/Ni NPs and zeolite. This confirms that the presence of zeolite as a support material caused the dispersion and stabilization of nanoparticles and further enhanced the reactivity of Fe/Ni NPs. Due to an increase in the surface area, active sites, and large formation of  $\cdot OH$  free radical in the low amount of  $H_2O_2$  concentration [6,31]. When using the Fenton-like oxidation processes, the decolorization rates were much higher. Additionally,  $\cdot OH$  free radicals are formed when  $Fe^0$  on the surface of GT-Z-Fe/Ni or Z-Fe/Ni reacts with  $H_2O_2$  to produce  $Fe^{+2}$ . When  $Fe^{+2}$  is oxidized by  $H_2O_2$  and converted into  $Fe^{+3}$ , it accelerates the breakdown of  $H_2O_2$  and produces highly reactive hydroxyl free radicals. Furthermore, when  $Fe^{+3}$  reacts with  $H_2O_2$ , it produces fewer reactive hydroperoxyl radicals ( $HOO\cdot$ )-OH[32]. In order to maintain a cycle for the generation of  $\cdot OH$  free radical in severe reactions continuing,  $Fe^{+3}$  is reduced to  $Fe^{+2}$ . Finally, the RR120 dye molecules on the surface of GT-Z-Fe/Ni or Z-Fe/Ni are attacked by  $\cdot OH$  free radical, resulting in RR120 dye degradation into  $CO_2$  and  $H_2O$ . Figure 15 reveals the absorption spectrum of RR120 dye before and after treatment at the optimum conditions.

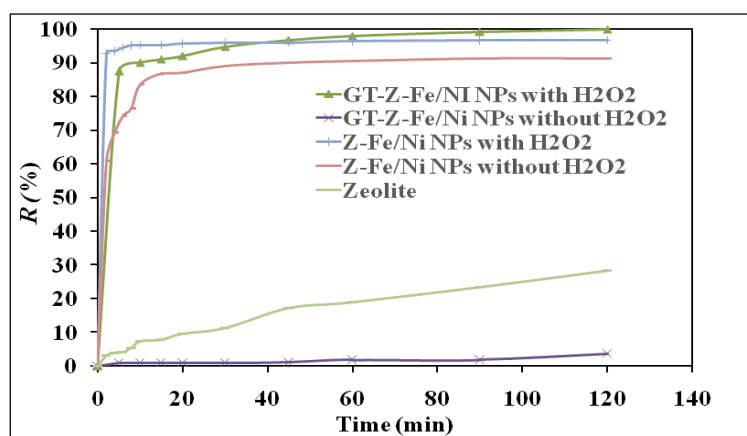


**FIGURE 14** Comparison between decolorization efficiencies of RR120 dye solution by Fenton-like and adsorption process without using  $H_2O_2$  using various catalysts under optimum condition after 120 minute at room temperature

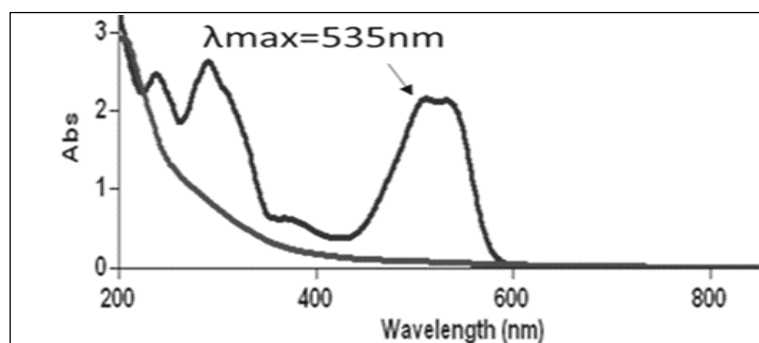


**FIGURE 15** The absorption spectrum of RR120 dye before and after treatment at the optimum conditions

**TABLE 6** The decolorization efficiencies of RR120 dye (25 mg/L) and optimum conditions by Fenton-Like and adsorption process at room temperature

Catalysts	The Concentration of RR120 dye (mg/L) After 120 (min) Reaction	Decolorization Efficiencies (%)	The Optimum Conditions
GT-Z-Fe/Ni with H <sub>2</sub> O <sub>2</sub>	0.024	99.90	[RR120 dye]=25 mg/L [H <sub>2</sub> O <sub>2</sub> ]=1mmol/L NPs dosage=0.1 g/L pH=3
GT-Z-Fe/Ni without using H <sub>2</sub> O <sub>2</sub>	24.66	6.33	[RR120 dye]=25 mg/L NPs dosage=0.1 g/L pH=3
Z-Fe/Ni with H <sub>2</sub> O <sub>2</sub>	0.86	96.65	[RR120 dye]=25 mg/L [H <sub>2</sub> O <sub>2</sub> ]=7.5 mmol/L NPs dosage=0.5 g/L pH=3
Z-Fe/Ni without using H <sub>2</sub> O <sub>2</sub>	2.24	91.26	[RR120 dye]=25 mg/L NPs dosage=0.5 g/L pH=3
Zeolite	18.38	28.25	[RR120 dye]=25 mg/L Zeolite dosage=0.5 g/L pH=3

## Conclusion

Green synthesis is another eco-friendly approach which avoids the use of harmful chemicals. Because of its low cost and great efficiency for industrial large-scale production, the green synthetic method is a new technique which can be applied to the synthesis of iron nanoparticles in the field of nanotechnology. In this research, bimetallic GT-Z-Fe/Ni and Z-Fe/Ni nanoparticles were synthesized by the green and chemical method in a suitable ratio of Fe/Ni using green tea leaf extract in an environmentally sustainable way and sodium borohydride as a reducing agent. Zeolite type 5A was prepared

by using the hydrothermal method, and then it was used as supporting materials on bimetallic Fe/Ni NPs. The best ratio obtained for (zeolite: Fe: Ni) of 2:1:0.2 (w/w) and it was used to synthesize NPs. The NPs were characterized using various techniques and were used as heterogeneous Fenton-like catalyst kinetics for the decolorization of RR 120 dye from aqueous media. The purpose of zeolite supporting Fe/Ni nanoparticles was to improve the reaction of nanoparticles, reduce the cost, and enhance the adsorption capacity for nanoparticles. The effects of various experimental conditions parameters such as H<sub>2</sub>O<sub>2</sub> concentration, reaction time, catalyst dosages, solution pH, the concentration of



(RR120) dye, and temperature effect were studied to determine an optimization method for removal. This study reveals that improvement was achieved when using GT-Z-Fe/Ni NPs and Z-Fe/Ni NPs to remove the dye solution. Under the optimum conditions, high decolorization efficiencies of RR120 dye (99.9% and 96.6%, respectively) were obtained by using GT-Z-Fe/Ni NPs and Z-Fe/Ni NPs to catalyze the Fenton-like oxidation. The experimental kinetic and thermodynamic parameter data showed that the degradation of RR120 dye by a Fenton-like oxidation process using GT-Z-Fe/Ni and Z-Fe/Ni nanoparticles fitted the (second-order and BMG) models well and that the process is appropriate for spontaneous reaction and endothermic reaction for all prepared nanoparticles. Subsequently, using green and chemical Fenton-like systems, a possible mechanism was determined for the oxidative degradation of RR120 dye. It demonstrates that GT-Z-Fe/Ni or Z Fe/Ni catalyzes H<sub>2</sub>O<sub>2</sub> activation, resulting in the formation of OH radicals and the degradation of the RR120 dye into CO<sub>2</sub> and H<sub>2</sub>O. The result illustrated that GT-Z-Fe/Ni and Z Fe/Ni NPS improvement and had excellent azo dye removal capabilities; however, it is preferred the catalyst synthesis by green methods to reduce and avoid the use of harmful chemicals.

### Acknowledgements

Great thanks to Almighty Allah, who awarded me the strength, I praise him and thank him for his grace and from him on me... I would like express high thanks to the Department of chemistry at the College of Science for women/ University of Baghdad, Iraq, and the Environment and Water Directorate /Ministry of Science and Technology, Iraq, for providing all the facilities to carry out this work.

Maysoon M. Abdul Hassan:

<https://orcid.org/0000-0002-4083-5470>

### References

- [1] N. Akhtar, M.I.S. Ishak, S.A. Bhawani, K. Umar, *Water*, **2021**, 13, 2660. [[Crossref](#)], [[Google Scholar](#)], [[Publisher](#)]
- [2] A.A. Mohammed, K.H. Ahmed, M.L. Imad, *Nat. Environ. Pollut. Technol.*, **2022**, 21, 355-365. [[Crossref](#)], [[Google Scholar](#)], [[PDF](#)]
- [3] S. Homaeigohar, *Nanomaterials*, **2020**, 10, 295. [[Crossref](#)], [[Google Scholar](#)], [[Publisher](#)]
- [4] K.G. Ahila, B. Ravindran, V. Muthunayanan, D.D. Nguyen, X.C. Nguyen, S.W. Chang, V.K. Nguyen, C. Thamaraiselvi, *Sustainability*, **2021**, 13, 329. [[Crossref](#)], [[Google Scholar](#)], [[Publisher](#)]
- [5] H. Xiang, G. Ren, Y. Zhong, D. Xu, Z. Zhang, X. Wang, X. Yang, *Nanomaterials Article*, **2021**, 8, 330. [[Crossref](#)], [[Google Scholar](#)], [[Publisher](#)]
- [6] A.K. Hassan, G.Y. Al-Kindi, G. Dalal, *Water Sci. Eng.*, **2020**, 13, 286-298. [[Crossref](#)], [[Google Scholar](#)], [[Publisher](#)]
- [7] A.K. Hassan, M.R. Mohammad, C. Gautam, N. Ravi, *Environ. Technol. Innov.*, **2019**, 15, 100380. [[Crossref](#)], [[Google Scholar](#)], [[Publisher](#)]
- [8] N. Beheshtkhoo, M.A.J. Kouhbanani, A. Savardashtaki, A.M. Amani, S. Taghizadeh, *Appl. Phys. A.*, **2018**, 124, 363. [[Crossref](#)], [[Google Scholar](#)], [[Publisher](#)]
- [9] H.Q. Alijani, S. Pourseyedi, M. Torkzadeh-Mahani, A. Seifalian, M. Khatami, *Artificial Cells, Nanomed. Biotechnol.*, **2020**, 48, 242-251. [[Crossref](#)], [[Google Scholar](#)], [[Publisher](#)]
- [10] K. Sravanthi, D. Ayodhya, P.S. Yadgiri, *J. Anal. Sci. Technol.*, **2018**, 9, 3. [[Crossref](#)], [[Google Scholar](#)], [[Publisher](#)]
- [11] T. Bao, J. Jin, M.M. Dantie, K. Wu, Z.M. Yu, L. Wang, J. Chen, Y. Zhang, R.L. Frost, *J. Saudi Chem. Soc.*, **2019**, 23, 864-878. [[Crossref](#)], [[Google Scholar](#)], [[Publisher](#)]
- [12] G. Gopal, H. Sankar, C. Natarajan, A. Mukherjee, *J. Environ. Manage.*, **2020**, 254, 109812. [[Crossref](#)], [[Google Scholar](#)], [[Publisher](#)]

- [13] G.G. Valiyeva, I Bavasso, L. Di Palma, S.R. Hajiyeva, M.A. Ramazanov, F.V. Hajiyeva. *Nanomaterials*, **2019**, *9*, 1130. [[Crossref](#)], [[Google Scholar](#)], [[Publisher](#)]
- [14] N. Ezzatahmedi, *J. Clean. Prod.*, **2019**, *151*, 21-33. [[Crossref](#)], [[Google Scholar](#)], [[Publisher](#)]
- [15] H. Yin Hai, L. Hai, D. Yingbo, L. Bing, W. Liang, C. Shangye, L. Mingke, L. Junfei, *Chem. Eng. J.*, **2018**, *347*, 664-681. [[Crossref](#)], [[Google Scholar](#)], [[Publisher](#)]
- [16] A.N. Hammadi, I.K. Shakir, *Iraqi J. Chem. Pet. Eng.*, **2019**, *20*, 27-33. [[Crossref](#)], [[Google Scholar](#)], [[Publisher](#)]
- [17] N. Butterfield, P.M. Rowe, E. Stewart, D. Roesel, S. Neshba, *J. Geophys. Res. Atmos.*, **2017**, *122*, 3023-3041. [[Crossref](#)], [[Google Scholar](#)], [[Publisher](#)]
- [18] K.Y. Abdolmotalleb, A. Seidmohammadi, M. Khazaei, A. Bhatnagar, M. Leili, *J. Environ. Health Sci. Engineer.*, **2019**, *17*, 337-351. [[Crossref](#)], [[Google Scholar](#)], [[Publisher](#)]
- [19] S. Mourdikoudis, R.M. Pallares, N.T.K. Thanh, *Nanoscale*, **2018**, *10*, 12871-12934. [[Crossref](#)], [[Google Scholar](#)], [[Publisher](#)]
- [20] A.R. Suvarna, A. Shetty, S. Anchan, N. Kabeer, S. Nayak, *Bionanoscience*, **2020**, *10*, 606-617. [[Crossref](#)], [[Google Scholar](#)], [[Publisher](#)]
- [21] H.M. Abd El-Aziz, R.S. Farag, S.A. Abdel-Gawad, *Nanotechnol. Environ. Eng.*, **2020**, *5*, 1-9. [[Crossref](#)], [[Google Scholar](#)], [[Publisher](#)]
- [22] X. Li, Y. Zhao, B. Xi, X. Mao, B. Gong, R. Li, X. Peng, H. Liu, *Appl. Surf. Sci.*, **2016**, *370*, 260-269. [[Crossref](#)], [[Google Scholar](#)], [[Publisher](#)]
- [23] Y.-C. Chiang, W.-T. Chin, *Nanomaterials*, **2022**, *12*, 1492. [[Crossref](#)], [[Google Scholar](#)], [[Publisher](#)]
- [24] A.R. Puthukkara, S. Jose, D. Lal, *J. Environ. Chem. Eng.*, **2020**, *9*, 104569. [[Crossref](#)], [[Google Scholar](#)], [[Publisher](#)]
- [25] H.M. Abdel-Aziz, R.S. Farag, S.A. Abdel-Gawad, *Int. J. Environ. Res.*, **2019**, *13*, 843-852. [[Crossref](#)], [[Google Scholar](#)], [[Publisher](#)]
- [26] G.Y.B. Al Kindi, A.K. Hassan, G.Y. Dalal, A.A. Husam, *IOP Conf. Ser.: Earth Environ. Sci.*, **2021**, *779*, 012092. [[Crossref](#)], [[Google Scholar](#)], [[Publisher](#)]
- [27] X. Wang, C. Jiang, B. Hou, Y. Wang, C. Hao, J. Wu, *Chemosphere*, **2018**, *206*, 587-596. [[Crossref](#)], [[Google Scholar](#)], [[Publisher](#)]
- [28] G.Y. AL-Kindi, F.H. AL Ani, *J. Eng. Technol.*, **2019**, *37*, 175-85. [[Crossref](#)], [[Google Scholar](#)], [[Publisher](#)]
- [29] P. Ma, Q. Liu, P. Liu, H. Li, X. Han, L. Liu, W. Zou, *J. Dispers. Sci. Technol.*, **2020**, *42*, 1350-1367. [[Crossref](#)], [[Google Scholar](#)], [[Publisher](#)]
- [30] D.F. Romdhane, Y. Satlaoui, R. Nasraoui, A. Charef, R. Azouzi, *J. Chem.*, **2020**, *2020*, 1-17. [[Crossref](#)], [[Google Scholar](#)], [[Publisher](#)]
- [31] D.V. Kerkez, S.C. Toma, G. Kozma, M.R. Be Celic Tomin, M.D. Prica, S.D. Roncevic, A.C. Kukovecz, B.D. Dalmacija, Z. Konya, *J. Taiwan Inst. Chem. Eng.*, **2014**, *45*, 2451-2461. [[Crossref](#)], [[Google Scholar](#)], [[Publisher](#)]
- [32] Z. Chi, Z. Wang, H.Q. Chu, P. Bin, L. Lucian, *RSC Adv.*, **2017**, *7*, 44605-44613. [[Crossref](#)], [[Google Scholar](#)], [[Publisher](#)]

**How to cite this article:** Maysoon M. Abdul Hassan\*, Sahar S. Hassan, Ahmed K. Hassan. Green and chemical synthesis of bimetallic nanoparticles (Fe/Ni) supported by zeolite 5A as a heterogeneous Fenton-like catalyst and study of kinetic and thermodynamic reaction for decolorization of reactive red 120 dye from aqueous pollution. *Eurasian Chemical Communications*, 2022, 4(11), 1062-1086. **Link:** [http://www.echemcom.com/article\\_152379.html](http://www.echemcom.com/article_152379.html)